Atmos. Chem. Phys., 13, 4203–4222, 2013
www.atmos-chem-phys.net/13/4203/2013/
doi:10.5194/acp-13-4203-2013

Atmospheric Chemistry and Physics Open Access

Aerosol pollution potential from major population centers

D. Kunkel[1,*], **H. Tost**[2], **and M. G. Lawrence**[1,**]

[1]Max Planck Institute for Chemistry, P.O. Box 3020, 55020 Mainz, Germany
[2]Johannes Gutenberg-University, Institute for Atmospheric Physics, 55099 Mainz, Germany
[*]now at: Johannes Gutenberg-University, Institute for Atmospheric Physics, 55099 Mainz, Germany
[**]now at: Institute for Advanced Sustainability Studies, 14467 Potsdam, Germany

Correspondence to: D. Kunkel (dkunkel@uni-mainz.de)

Received: 6 August 2012 – Published in Atmos. Chem. Phys. Discuss.: 25 September 2012
Revised: 15 March 2013 – Accepted: 20 March 2013 – Published: 19 April 2013

Abstract. Major population centers (MPCs), or megacities, represent the largest of growing urban agglomerations with major societal and environmental implications. In terms of air quality, they are seen as localized but strong emission sources of aerosols and trace gases which in turn affect air pollution levels in the city or in downwind regions. In the state-of-the-art atmospheric chemistry general circulation model EMAC, generic aerosol and gas-phase tracers with equal emission source strengths at 46 MPC locations are used to study the balance between local pollution build-up and pollution export, either vertically into the upper troposphere or horizontally in the lower troposphere. The insoluble gas-phase tracers with fixed lifetimes are transported with the atmospheric circulation, while the aerosol tracers also undergo gravitational sedimentation as well as dry and wet deposition processes. The strength of low-level tracer export depends on the location of the emission source and prevailing meteorology, in particular on atmospheric stability and the height of the boundary layer and the mixing out of this layer. In contrast, vertical transport of tracer mass depends on the tracer's solubility: the more soluble a tracer is, the less mass reaches altitudes above five kilometers. Hence, the mass of insoluble gas-phase tracer above five kilometers can be up to ten times higher than the hydrophilic aerosol mass from the same source. In the case of aerosol tracers, pollution build-up around the source is determined by meteorological factors which have only indirect effects on tracer lifetime, like surface wind, boundary layer height, and turbulent mixing, as well as those which affect the lifetime of the tracers such as precipitation. The longer a tracer stays in the atmosphere, the lower is the relative importance of the location of the source to the atmospheric mass, and thus the lower is the relative local pollution build-up. We further use aerosol deposition fields to estimate regions with high deposition, that is more than 1 % or more than 5 % of the corresponding tracer emission deposited in this region. In doing so, we find that the high deposition areas are larger for aerosols with diameters of 10.0 µm, and these differ less between the MPCs than for aerosols with diameters smaller than 2.5 µm due to faster deposition. Furthermore, cities in regions with high precipitation rates or unfavorable geographic locations, e.g., in a basin, suffer most of this high deposition. Most of the high deposition occurs over land, although about 50 % of the MPCs are located along coastlines. By folding the aerosol deposition fields with geographical distributions of cropland, pasture, and forest, the impact on different land ecosystems is assessed. In general, forest is exposed most to deposition from MPCs while pastureland is least affected. Moreover, the impact on humans, measured with a threshold exceedance of pollutant surface mixing ratios, is more dependent on population densities than on the size of the area with a certain mixing ratio.

1 Introduction

One of the big challenges of the future is the sustainable growth of urban agglomerations. Since 2008 the majority of human population lives in urban regions, with the prospect that the trend of human inflow into urban areas will continue throughout this century. The largest of these agglomerations, so-called megacities or major population centers (MPCs), have two faces. They often develop much faster than the country in which they are located in and promote human

development as well as generation of knowledge, technology, and wealth (Kraas, 2007). Furthermore, they can offer a significant chance for climate mitigation strategies, as the per capita emission is smaller when many people live close together (Parrish et al., 2009). However, these human agglomerations are very heterogeneous with respect to possible lifestyle of different groups, and consequently manifest different awareness in the handling of energy, water, and waste. Moreover, both increased residential housing as well as the clustering of industry in these metropolitan areas lead to the strong localized release of air pollutants, which substantially contributes to a decrease in air quality for local dwellers as well as in regions downwind (Molina and Molina, 2004). The urban growth occurs on less than 3 % of the land surface but with global consequences (Grimm et al., 2008). The enduring urbanization leads to major changes in land cover and land use with subsequent changes in surface mean temperatures (Kalnay and Cai, 2003).

There has been considerable research on these impacts on local to regional (e.g., Parrish et al., 2009, 2011) and global (e.g., Lawrence et al., 2007; Butler and Lawrence, 2009; Butler et al., 2012) scales, as well as several large megacity projects (e.g., Baklanov et al., 2010; Molina et al., 2010). Lawrence et al. (2007, later referred to as L07) studied the outflow characteristics of generic gas-phase tracers with three different lifetimes (1, 10, 100 days) from 36 MPCs to obtain insight into the balance between local pollution build-up and long-range transport. They found that low-level export is strongest in middle and high latitudes, while export into the free troposphere is dominant in the tropics. Moreover, vertical mixing is most responsible for reducing the surface pollution. They provide detailed insight in the outflow characteristics of the gas-phase tracers, but with a limited range of tracer properties. This study picks up where L07 left off and answers the following questions:

1. How robust are the results of L07, or do they depend strongly on the selected model?

2. To what degree do outflow characteristics depend on the lifetime of the tracer, especially if it varies in space and time, and how does it differ for gaseous and aerosol substances?

3. What more can be learned from tracer distributions and from tracer deposition fields when they are convolved with geographical population or agricultural distributions?

To investigate these aspects we use the global 3-D state-of-the-art atmospheric chemistry general circulation model (AC-GCM) EMAC (ECHAM5-MESSy Atmospheric Chemistry, Jöckel et al., 2006) with generic aerosol tracers of various sizes and different solubility as well as generic gas-phase tracers equal to those used by L07. 46 cities around the world (see Table 1) have been chosen as emission hotspots to determine the balance between pollutant build-up around the source and pollutant export.

In Kunkel et al. (2012) the same set of MPCs was used to determine the remote aerosol deposition potential, i.e., the deposition beyond various distances. In particular, it was found that on average about half of the emitted mass of small ($d \leq 2.5\,\mu m$) aerosol tracers is deposited beyond 1000 km. Several other studies investigated trace gas or aerosol transport from various, mostly larger sources such as countries or even continents on continental scales (e.g., Duncan and Bey, 2004; Park et al., 2005; Wagstrom and Pandis, 2010) or transcontinental scales (e.g., Betzer et al., 1988; Jaffe et al., 1999; Wild and Akimoto, 2001; Stohl et al., 2002, 2003; Liu and Mauzerall, 2007; Liu et al., 2009). More studies concerning pollutant dispersion from smaller emission points have been published for the regional scale, commonly focusing on one source point either for different meteorological conditions or with changed emission scenarios (e.g., de Foy et al., 2006; Streets et al., 2007; Wang et al., 2010; Song et al., 2010). In this study, as well as for L07, Butler et al. (2008), and Kunkel et al. (2012), the focus is directly on the comparison between MPCs all over the world.

We structured the paper to first provide a description of the EMAC model system, the metrics to characterize the outflow, and further data on population and agricultural distributions. In Sect. 3 we briefly compare EMAC results with results from L07 to assess the robustness of their analysis before the aerosol dispersion is discussed in Sect. 4. The aerosol tracers are then compared to generic gas-phase tracers in Sect. 5, and finally in Sect. 6 the aerosol deposition and surface densities are used to assess the impact of MPCs on agriculture and population. The key conclusions and further open questions are summarized in the last section.

2 Model and analysis data

2.1 Model and major population centers

This study uses the same setup as Kunkel et al. (2012) with 46 major population centers distributed around the world, as listed in Table 1. Not all of them strictly fulfill the criteria to be called a megacity, for which, depending on the definition, either more than five or ten million inhabitants are needed (UNFPA, 2007). However, we use several additional cities, e.g., Johannesburg, Sydney, Melbourne, Atlanta, Kinshasa, Khartoum, and Nairobi, due to their outstanding importance in their region or because they are expected to become megacities in the near future. Furthermore, we include three areas, i.e., the Rhine–Ruhr area, the Po Valley, and the Szechuan Basin, which are agglomerations of many cities and important industrial sites. Moreover, Hong Kong includes also the Pearl River Delta (PRD), and Kinshasa in the Democratic Republic of the Congo is a representative for for agglomeration together with Brazzaville in the

Table 1. Name, location, and climate class of all MPCs used as urban point sources. Longitude and latitude correspond to the model grid box with tracer emissions. DRC = Democratic Republic of the Congo, RC = Republic of the Congo, PRC = People's Republic of China, ROK = Republic of Korea. Climate classes from Peel et al. (2007): Am = tropical, monsoon; Aw = tropical, savannah; BWh = arid, desert, hot; BSk = arid, steppe, cold; Csa = temperate, dry, hot summer; Csb = temperate, dry, warm summer; Cwa = temperate, dry winter, hot summer; Cwb = temperate, dry winter, warm summer; Cfa = temperate, no dry season, hot summer; Cfb = temperate, no dry season, warm summer; Dfa = cold, no dry season, hot summer; Dfb = cold, no dry season, warm summer; and Dwa = cold, dry winter, hot summer.

MPC	Long.	Lat.	Climate class
Europe			
London, UK	−0.08	51.50	Cfb
Paris, France	2.33	48.83	Cfb
Rhine-Ruhr, Germany	7.00	51.50	Cfb
Moscow, Russia	37.62	55.75	Dfb
Po Valley, Italy	11.00	45.00	Cfa
Rome, Italy	12.30	41.50	Csa
Athens, Greece	23.40	37.60	Csa
Istanbul, Turkey	29.00	41.00	Csa
Africa			
Cairo, Egypt	31.25	30.03	BWh
Khartoum, Sudan	32.50	15.50	BWh
Nairobi, Kenya	36.80	−1.27	Cwb
Kinshasa, DRC, Brazzaville, RC	15.30	−4.33	Aw
Lagos, Nigeria	3.45	6.42	Aw
Johannesburg, South Africa	28.93	−26.52	Cwb
West Asia			
Baghdad, Iraq	44.70	33.33	BWh
Teheran, Iran	51.42	35.68	BWh
South Asia			
Karachi, Pakistan	67.07	24.85	BWh
Mumbai, India	72.90	18.92	Aw
Dehli, India	77.20	28.63	Cwa
Kolkata, India	88.40	22.57	Aw
Dhaka, Bangladesh	90.43	23.72	Aw
East Asia			
Szechuan Basin, PRC	105.00	30.00	Cwa
Hong Kong, PRC	114.20	22.20	Cwa
Beijing, PRC	116.40	39.92	Dwa
Tianjin, PRC	117.15	39.15	Dwa
Shanghai, PRC	121.48	34.25	Cfa
Seoul, ROK	127.10	37.52	Cwa
Osaka, Japan	135.45	34.65	Cfa
Tokyo, Japan	138.75	35.67	Cfa
South East Asia			
Bangkok, Thailand	100.50	13.70	Aw
Manila, Philippines	121.50	14.50	Aw
Jakarta, Indonesia	106.83	−6.20	Am
Oceania			
Melbourne, Australia	145.00	−38.00	Cfb
Sydney, Australia	151.20	−33.87	Cfa
North America			
Los Angeles, USA	−118.28	34.05	BSk
Chicago, USA	−87.67	42.00	Dfa
Houston, USA	−95.30	29.75	Cfa
Atlanta, USA	−84.50	33.00	Cfa
New York,USA	−74.02	40.72	Cfa
Mexico City, Mexico	−99.02	19.43	Cwb
South America			
Lima, Peru	−77.03	−12.03	BWk
Bogotá, Columbia	−74.20	4.40	Cfb
Santiago, Chile	−70.67	−33.50	Csb
Buenos Aires, Argentina	−58.33	−34.58	Cfa
São Paulo, Brazil	−46.62	−23.63	Cfa
Rio de Janeiro, Brazil	−43.20	−22.92	Aw

Republic of the Congo. All MPCs are taken as large emission point sources for generic tracers to study the dispersion in the atmosphere, and in the case of aerosol tracers subsequent deposition onto the surface. For this we apply the AC-GCM EMAC (Jöckel et al., 2006) with ECHAM5 (version 5.3.01, Roeckner et al., 2006) as a base model to calculate the meteorology. The base model is coupled to the Modular Earth Submodel System (MESSy, version 1.9, Jöckel et al., 2005, and http://www.messy-interface.org), which allows the inclusion of different sub-models for physical and chemical processes in the atmosphere and interactions between the atmosphere and biosphere. The model provides a good representation of gas-phase tracers (e.g., Jöckel et al., 2006; Pozzer et al., 2010; Tost et al., 2007) as well as aerosols (e.g., Pringle et al., 2010; Pozzer et al., 2012). Generic aerosol tracers have been used by Burrows et al. (2009) to study the transport of biogenic aerosol particles between different ecosystems and by Lelieveld et al. (2012) to determine the global exposure risk after nuclear accidents.

2.1.1 Meteorological setup

The model resolution was chosen to be T106L31, that is a triangular truncation at wave number 106 for the spectral core of ECHAM5 (T106), and with 31 hybrid sigma-pressure levels in the vertical (L31), mainly distributed in the troposphere from the surface up to 10 hPa. The chosen spectral resolution corresponds to a quadratic Gaussian grid of about $1.125° \times 1.125°$, or $\sim 100\,\text{km} \times 100\,\text{km}$ in longitude and latitude, respectively. This is a relatively high spatial resolution for global model simulations, but still a low resolution compared to what would be needed to simulate individual megacities. Therefore, the details of megacities or the concentration

fields within the megacities are not considered here; rather, the megacities represent large point sources for examining the long-range transport.

The model simulations were initialized in July 2004 and ended in January 2006, with the first half a year used as model spin-up time. Meteorological variables, namely temperature, vorticity, divergence, and the logarithm of surface pressure are weakly nudged towards analysis data from the ECMWF ERA-Interim reanalysis project (Dee et al., 2011). The year 2005 was chosen as analysis time period as it shows no strong annual modes in ENSO or NAO and coincides with the main analysis year of the MEGAPOLI project (Baklanov et al., 2010).

2.1.2 MESSy setup

The present model study comprises the following physical processes: emission, atmospheric transport, and wet and dry deposition of generic aerosol tracers and emission, atmospheric transport, and a radioactive-like decay of generic gas-phase tracers equal to those used in L07. For each of the 46 emission points, an independent set of tracers was released at a constant, prescribed emission rate of $1\,\mathrm{kg\,s^{-1}}$. The emission was placed in the middle of the lowest model layer in all grid boxes hosting an MPC. These boxes have a mean depth of about 60 m in the vertical and approximately 100 km in the horizontal. Pozzer et al. (2009) found that the emission height affects tropospheric chemistry close to the source if the emissions are within the planetary boundary layer; the overall effect on the chemical composition is rather low. However, potential transport distances might increase with injections into the free troposphere, e.g., from industrial stacks. Thus, by using surface emissions, we obtain a conservative estimate for results regarding long-range transport.

Tracer transport is split into transport by large-scale advection (Lin and Rood, 1996), which is to a large extent resolved in the global model, and by sub-grid-scale convection (Tiedtke, 1989; Nordeng, 1994; Lawrence and Rasch, 2005; Tost et al., 2010), vertical diffusion by turbulent mixing (Roeckner et al., 2006), and in the case of aerosols gravitational settling (Kerkweg et al., 2006a), neglecting chemical reactions and micro-physical changes. The atmospheric residence time of the aerosol tracers is determined only by four independent removal processes: (1) aerosol sedimentation onto the surface, (2) dry deposition by contact with the surface based on its roughness and the boundary layer mixing (Kerkweg et al., 2006a), and scavenging by (3) impaction and (4) nucleation in large-scale and convective clouds (Tost et al., 2006, 2010). We refer to (1) and (2) as dry deposition processes and to (3) and (4) as wet deposition processes. MESSy sub-models in use for this study are CLOUD (Jöckel et al., 2006), CONVECT and CVTRANS (Tost et al., 2010), RAD4ALL (Jöckel et al., 2006), ONLEM (Kerkweg et al., 2006b), DRYDEP (Kerkweg et al., 2006a), SEDI (Kerkweg et al., 2006a), SCAV (Tost et al., 2006, 2007), and PTRAC (Jöckel et al., 2008).

In this study monomodal aerosol tracers represent aerosols with ambient diameters of 0.1, 0.5, 1.0, 2.5, and 10.0 µm with a fixed standard deviation of 1.0. Instead of using a complex, computationally expensive aerosol module to explicitly treat aerosol micro-physics, we use two different aerosol solubility states which differ in the treatment of scavenging by nucleation: in one case all aerosols can undergo this process (further denoted as $\mathrm{NS_{act}}$) which is tracer size dependent, and in the other case this process is completely inhibited and the aerosol tracers are considered to be insoluble (further denoted as $\mathrm{NS_{inact}}$), which is summarized in Table 2. These two aerosol states are considered as extrema with respect to aerosol solubility, representing an upper and lower estimate of results with the range in between being representative for most of the real atmospheric aerosol particles and consequently their chemical composition and reactivity. Thus, ten aerosol tracers are released at each emission source point, one for each size and solubility state, all with the same source strength. This allows us to use the various aerosol tracer properties to obtain information on various parts of the aerosol size distribution. In total, we use a set of 460 aerosol tracers (46 source points $\times$ 5 aerosol sizes $\times$ 2 aerosol solubility states) which do not interact with each other and have no feedbacks on clouds or the radiative balance. Interpretation of the sizes is the same as that described in Kunkel et al. (2012).

Figure 1 shows the different annual atmospheric residence times of the tracers, ordered by the longest lifetime of the $\mathrm{NS_{inact}}$ 1 µm aerosol tracers. The aerosol residence time is calculated with a steady state approach by dividing the annual mean aerosol load by the total annual emission (Seinfeld and Pandis, 2006). We obtain residence times for each MPC with an upper limit provided by $\mathrm{NS_{inact}}$ and a lower limit by $\mathrm{NS_{act}}$ aerosol tracers. As the latter are more susceptible to wet deposition, they have shorter atmospheric residence times. 80 to 95% of the mass of fine aerosols is wet deposited, which is the main sink of fine aerosols in nature and in the model (Monks et al., 2009; Kunkel et al., 2012). All aerosol tracers with diameter $d \leq 2.5\,\mu\mathrm{m}$ are defined as fine aerosols, similar to the definition of $\mathrm{PM_{2.5}}$, which is the mass of aerosols with an ambient diameter less than 2.5 µm. For larger aerosols the difference in residence time with respect to aerosol solubility becomes smaller as dry and wet deposition contribute almost equally to the sink processes (Kunkel et al., 2012). Furthermore, the effect of nucleation scavenging is smaller for larger particles as they are removed very efficiently by impaction scavenging (Tost et al., 2006). In the following chapters we will refer to aerosol tracers with 0.1, 0.5, and 1.0 µm diameters as small aerosol tracers, and to those with 10.0 µm diameters as coarse aerosol tracers.

Table 2. Brief description of symbols used in this study.

Symbol	Description
NS_{act}	Aerosol tracers which can be scavenged by nucleation
NS_{inact}	Aerosol tracers which cannot be scavenged by nucleation
$RCL_{0.5\,km}$	Fraction of total tracer mass retained in a circular volume of height 0.5 km and a radius of 500 km
$ELR_{1.0\,km}$	Fraction of total tracer mass exported beyond 1000 km and below an altitude of 1.0 km
E_{UT}	Fraction of total tracer mass above 5 km altitude
A_Y	Total surface area (in $10^6\,km^2$) of model grid cells with a tracer mass larger than Y = 10 ng m^{-3}
DEP_{accu}	Annual mean deposition mass flux in kg m^{-2} s^{-1}
EM_{total}	Annual global mean emission flux in kg m^{-2} s^{-1}
D_X	Emission normalized deposition fraction, i.e., the fraction of tracer DEP_{accu} in each grid cell which is larger than X per cent of the corresponding EM_{total}, where $X = 1$ or 5 %
A	Tropical climate class
B	Arid climate class
Cs	Temperate, dry summer climate class
Cw	Temperate, dry winter climate class
Cf	Temperate, no dry season climate class
D	Cold climate class

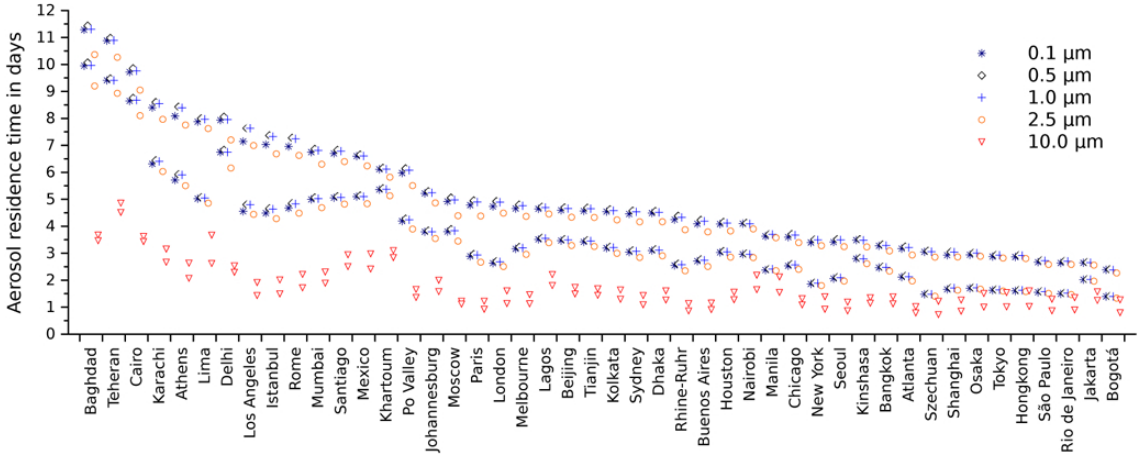

Fig. 1. Aerosol residence times for all MPCs and all aerosol tracers. The upper value is determined by the NS_{inact} tracers, the lower value by the NS_{act} tracers.

2.2 Metrics

We use similar metrics to L07 to distinguish between pollution at low levels and in the upper troposphere, and also between local and remote pollution from MPCs (summarized in Table 2). The equal emission rate for all tracers and MPCs provides the potential to compare the pollution from urban centers only by their location and prevailing meteorology, independent of real emissions. The upper tropospheric pollution potential is characterized by the mass fraction above 5 km altitude (E_{UT}). The low-level pollution potential is split into a long-range ($ELR_{1\,km}$) and a city-scale ($RCL_{0.5\,km}$) fraction with $ELR_{1\,km}$ being the mass fraction below 1 km altitude and at least 1000 km away from the source, while $RCL_{0.5\,km}$ is the mass fraction retained in the first 500 km from the emission source points and below 0.5 km altitude. The first two metrics describe the outflow of an MPC, either vertically (E_{UT}) or quasi-horizontally ($ELR_{1\,km}$), the third one ($RCL_{0.5\,km}$) the pollution build-up around the source. To calculate $RCL_{0.5\,km}$ and $ELR_{1\,km}$, a set of equidistant points around each emission source have to be determined. On a plane they are located on a circle with the emission source as center point; on a graticule (latitude–longitude grid) this becomes an ellipsoid. The corresponding distances from the center points are based on the radii of the WGS84 ellipsoid (National Imagery and Mapping Agency, http://earth-info.nga.mil/GandG/publications/tr8350.2/wgs84fin.pdf, 2000 or see L07). In addition, the local pollution build-up can be

assessed by adding up the area, or other properties in this area, in which the tracer density exceeds a given threshold A_Y, with Y a threshold value in $\mathrm{ng\,m^{-3}}$ (tracer mixing ratios are provided in $\mathrm{mol\,mol^{-1}}$ and can be converted to $\mathrm{ng\,g^{-1}}$ with molar masses for the tracers, here chosen to be $1\,\mathrm{g\,mol^{-1}}$, and the molar mass of air $28.97\,\mathrm{g\,mol^{-1}}$; the surface air density, approximately $1\,\mathrm{kg\,m^{-3}}$, is then used to convert the mass mixing ratio in the lowest layer to a concentration in $\mathrm{ng\,m^{-3}}$).

We further focus on the concentrated deposition patterns, i.e., high relative deposition. We calculate the emission normalized deposition fraction D_X (in %), i.e., the annual mean deposition flux $\mathrm{DEP_{accu}}$ (in $\mathrm{kg\,m^{-2}\,s^{-1}}$) in each model grid box divided by the annual global mean emission flux $\mathrm{EM_{total}}$ (in $\mathrm{kg\,m^{-2}\,s^{-1}}$) from the corresponding source point:

$$D_X = \frac{\mathrm{DEP_{accu}}}{\mathrm{EM_{total}}} \times 100\,\%. \quad (1)$$

This fraction together with a threshold value X (in %) can be used to characterize the impact of an MPC on different ecosystems. We fold D_X with surface properties, namely total surface area, water or land area, cropland, pasture, or forest. Similarly, we use A_Y to assess the population number being exposed to a certain surface mixing ratio. Depending on the property, we speak of a cropland, pasture, or forest deposition or human exposure in the following sections.

Finally, it is noted that for seasonal analyses, metric results for urban centers from the Southern Hemisphere have been shifted by six months to match the seasons in the Northern Hemisphere.

2.3 Agricultural and population data

Gridded population numbers for the year 2005 are used to determine the impact of aerosols on humans (see also Fig. S1 in the Supplement). Data are based on gridded population data of more than 300 000 national and sub-national administrative units to assign population values to grid cells (SEDAC, 2005).

Moreover, the fractions of three different land ecosystems, cropland, pasture, and forest, are used to determine the impact on land ecosystems (see Fig. S1 in the Supplement). Cropland and pasture data are compiled using satellite-derived land-cover data and agricultural inventory data (Ramankutty et al., 2008) for the year 2000. Data is originally available at about 10 km horizontal resolution (http://www.geog.mcgill.ca/landuse/pub/Data/, as of 8 June 2012). The forest data is based on US Geological Survey Global Forest Resource Assessment (FRA 2000) and is based on images from the Advanced Very High Resolution Radiometer (AVHRR) satellite at a resolution of about one kilometer (http://edc2.usgs.gov/glcc/fao/index.php, as of 8 June 2012). The data set originally comprised five classes, closed forest (40–100 % canopy cover), open or fragmented forest (10–40 % canopy cover), other wooded land, and water (lakes, rivers, etc.), which have been merged into one forest class for this study.

All these data sets have been regridded to the model resolution, and together with the metrics D_X and A_Y are used to assess the human exposure, cropland deposition exposure, pasture deposition exposure, and forest deposition exposure.

Table 3. Differences between EMAC and MATCH-MPIC annual values and corresponding ranks for $\mathrm{ELR_{1\,km}}$, E_{UT}, and A_{10} for the 36 MPCs. $\bar{x}$, mean difference; x_{d}, corresponding mean absolute deviation; with $\bar{x} = \Sigma_{i=1}^{N} x_i/N$, $x_{\mathrm{d}} = \Sigma_{i=1}^{N} |x_i'|/N$, and $x_i' = x_i - \bar{x}$, where x_i is the metric value of an MPC and N is the total number of MPCs.

	$\mathrm{ELR_{1\,km}}$		E_{UT}		A_{10}	
	%	Rank	%	Rank	$\times 10^6\,\mathrm{km^2}$	Rank
$\bar{x}$	−2.32	0	1.05	0	−0.91	0
x_{d}	2.88	4.89	6.41	3.94	0.99	4.06

3 Model comparison of outflow characteristics from major population centers

We first summarize the results of the model comparison between the EMAC model and the MATCH-MPIC model, a semi-offline, three-dimensional chemical transport model (e.g., Rasch et al., 1997; Lawrence et al., 1999; Kuhlmann et al., 2003) which was used by L07. A more detailed analysis is given in the electronic Supplement. We use the same 36 major population centers as L07 to test the reproducibility of their results. Total and upper tropospheric column and surface densities agree well between the two simulations and also the resulting metrics give comparable numbers with high coefficients of determination (R^2) of about 0.75. In general, the low-level export is stronger when simulated with MATCH-MPIC, as well as the area with a mass threshold exceedance of $10\,\mathrm{ng\,m^{-3}}$, while the upper tropospheric pollution is stronger in EMAC (see Table 3).

The main results from L07 are well reproduced when using EMAC, which underlines the robustness of the results. Discrepancies in the metrics mainly result from the different underlying meteorological fields (from NCEP for MATCH-MPIC and from ECMWF for EMAC) and different advective and convective transport schemes which introduce the largest uncertainties in such calculations.

4 Atmospheric dispersion of aerosols from urban emission hotspots

In the following section we focus on aerosol transport with subsequent deposition which leads to different atmospheric residence times of single tracers. Aerosols are removed by dry and wet deposition processes, thus, aerosol weight,

surface properties as well as meteorological conditions determine the distance an aerosol particle can travel in the atmosphere before being deposited to the ground. We utilize $RCL_{0.5\,km}$ to characterize the local low-level pollution build-up, $ELR_{1\,km}$ for the remote low-level pollution, and E_{UT} for upper tropospheric pollution.

4.1 Local pollution build-up

In Fig. 2, the top panel shows annual averages of $RCL_{0.5\,km}$. The gray shaded area which is bounded by the solid and dashed black lines represents the MPC averages for NS_{inact} and NS_{act} aerosol tracers. The light gray shaded areas contiguous to this area denote the standard deviation, each plotted one-sided for the upper and lower bound. The overall annual mean values range between 10 to 14 % for small tracers and 15 to 19 % for large tracers. Six climate classes are used equal to those in Kunkel et al. (2012), to provide more information about regional differences. As our results are mainly dependent on the prevailing meteorology, the MPCs are grouped by their Köppen–Geiger climate classification (Peel et al., 2007), which depends on temperature and precipitation (see also Table 1): tropical, A (red); arid, B (brown); temperate, no dry season, Cf (light green); temperate, dry winter, Cw (light blue); temperate, dry summer, Cs (dark green); and cold, D (blue) (see Table 2).

For small NS_{inact} aerosol tracers, minimum retention of tracer mass occurs in urban centers in arid (B) and temperate dry summer (Cs) regions with $RCL_{0.5\,km}$ of about 7 %, and the maximum for MPCs in tropical (A) and cold (D) regions with values of about 11 to 12 %. The same regions show the minima for NS_{act} aerosol tracers of about 9 %, while tropical and temperate no dry season (Cf) means are the maxima, with values of about 17 %. Large aerosol tracers from urban centers in arid regions reveal minimum values of 9 % (NS_{inact}) and 10 % (NS_{act}), respectively, while the maximum values are found for both solubility states in cold regions and also in the soluble case for temperate no dry season regions, with climate class means of 20 % (NS_{inact}) and 22 % (NS_{act}). Further, almost all mean values for arid and temperate dry summer regions show, independent of solubility state, smaller mean values than all other climate class means, which can also be seen in almost every season of the year (see Fig. S4 in the Supplement). Only in temperate dry winter regions do low $RCL_{0.5\,km}$ values appear during winter months (DJF). Thus, the relative pollution build-up in these two regions is smaller than in all other climate classes. Furthermore, the pollution build-up in two contrary climate regions, tropical and cold, is highest, although meteorological conditions lead to different atmospheric dispersion (see Sect. 4.2).

The retention of tracer mass is controlled by two mechanisms. On the one hand, $RCL_{0.5\,km}$ anti-correlates with the atmospheric residence time of the tracers. As mentioned before, the residence time is mainly governed by wet removal, and thus aerosol tracers with short residence times often orig-

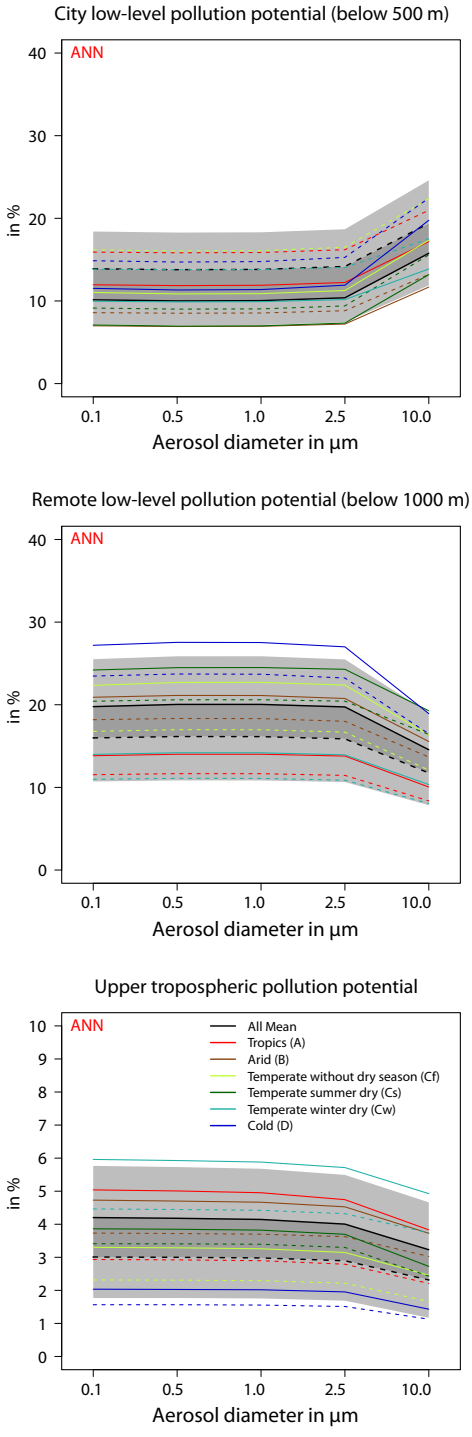

Fig. 2. Annual averages of $RCL_{0.5\,km}$ (upper panel), $ELR_{1\,km}$ (middle panel), and E_{UT} (bottom panel). Dark gray shaded areas represent the area between the total means (black lines) of NS_{act} (dashed) and NS_{inact} (solid) MPC tracers. Light gray shaded areas show one standard deviation, plotted single sided for NS_{act} and NS_{inact} mean values. Colored lines represent the mean values for different climate classes: tropical (red, A); arid (brown, B); temperate, no dry season (light green, Cf); temperate, dry summer (dark green, Cs); temperate, dry winter (light blue, Cw); and cold (blue, D).

inate in regions with high precipitation rates, i.e., tropical regions. In contrast, for tracers from arid regions the residence time is relatively long due to missing precipitation. Thus, the relative contribution of the emission to the global burden of a tracer is larger for those with short lifetimes, since a large fraction of the burden is generally closer to the source with higher $RCL_{0.5\,km}$ values. This accounts for about 50 % of the variance in the overall $RCL_{0.5\,km}$ results. On the other hand, meteorological conditions that change the distribution of the tracer mass in the atmosphere, though not directly their residence time, are responsible for the missing variance. For example, surface winds, turbulent mixing, or the depth of the boundary layer height can alter $RCL_{0.5\,km}$ values without affecting the aerosol lifetime.

The influence of precipitation also plays a major role in the seasonal variations in $RCL_{0.5\,km}$. The minimum climate means stay almost constant throughout the year since the minima are given by mean values from regions which are weakly affected by precipitation. In contrast, the maxima vary with the season, with the difference between $RCL_{0.5\,km}$ minima and maxima being largest in summer (JJA) when precipitation rates are generally larger and consequently the aerosol residence times shorter.

4.2 Outflow of pollution from urban centers

4.2.1 Remote low-level outflow

In contrast to local pollution build-up, the emissions from urban centers also undergo transport which can either be horizontal or vertical. We first assess the horizontal transport focusing on the mass which is transported near the surface or which was first lifted and subsequently descended again to lower altitudes, e.g., in a dry intrusion or simply by aerosol sedimentation. Overall annual means of $ELR_{1\,km}$ vary between 16 and 20 % for small tracers and 12 and 15 % for large tracers, with larger values now given by NS_{inact} aerosol tracers (see middle panel in Fig. 2). Including climate class means, the diversity increases with values ranging from 11 to 27 % for small and from 8 to 19 % for large aerosol diameters. Aerosol tracers from cold regions possess the largest remote low-level mass fraction with more than 25 % of their total mass (averaged over NS_{inact} and NS_{act} tracers) located in the near-surface layer downwind of the source. In contrast to the local build-up, aerosols from temperate dry summer regions show a large downwind pollution potential. The least export occurs in temperate dry winter and tropical regions as upper-level export is favored in these regions (see following Sect. 4.2.2).

Similarly, the smallest seasonal means appear for aerosol tracers from tropical regions, except during winter when those from temperate dry winter regions show the least downwind pollution potential due to relatively enhanced transport into the upper troposphere. $ELR_{1\,km}$ means peak for aerosol tracers from either cold or temperate dry summer regions. In general, the highest downwind pollution potential is found during winter months (DJF) with overall means between 21 and 25 %, and the least during summer (JJA) with overall means of about 10 to 12 %.

In winter, atmospheric low-level inversions occur more frequently, and aerosol tracer mass is kept more efficiently within the boundary layer, which is commonly shallower during this time of the year. Together with less convective activity, the $ELR_{1\,km}$ seems to be dominated by the atmospheric stability. Higher stability leads to greater remote low-level transport.

Similar to L07 we analyzed the response of a change in the depth of the near-surface layer and consider a metric height of 500 m. L07 found that the remote low-level export decreased almost linearly with the volume, i.e., only a tenth of the $ELR_{1\,km}$ numbers are found in a layer which is 100 m deep. For aerosols, on annual average we find that about 50 % of the $ELR_{1\,km}$ mass is present in a volume half as deep as our original volume, thus the same relationship is found for aerosols as for gases in L07. We see a small seasonal variation in this number with a maximum in winter (on average 53 %) and a minimum in summer (on average 47 %) due to the same reason as for the seasonal variation in $ELR_{1\,km}$. Additionally, the ratio is slightly dependent on aerosol solubility, with higher ratios for soluble aerosol tracers but with almost no dependence on aerosol size.

4.2.2 Outflow into the upper troposphere

Aerosol mass can also be lofted out of the source region into the upper troposphere, commonly by convective or frontal lifting depending on location and time of year (bottom panel of Fig. 2). Overall annual means of E_{UT} are between 3 and 4 % for small aerosol tracers and 2.5 and 3.5 % for large aerosol tracers, and thus much smaller than for the other two metrics and especially much smaller than E_{UT} values for gas tracers reported by L07. The order of the climate means is reversed compared to the order found for $ELR_{1\,km}$, now with maximum pollution for aerosol tracers from temperate dry winter and tropical regions and minimum pollution for those from cold regions.

These findings rely on several facts which need to be discussed. First, the difference between NS_{inact} and NS_{act} means strongly varies between climate classes. For tropical regions which are heavily and regularly affected by convection, the different treatment of nucleation scavenging leads to strong differences in the upper tropospheric pollution with NS_{act} means accounting for only about 60 % of the NS_{inact} means. In contrast, for aerosols from cold regions this ratio is about 90 %, and thus the difference is almost negligible, caused by an inefficient nucleation scavenging of snow and ice crystals according to the model formulation. Second, in L07 the strongest vertical tracer displacement occurred in tropical regions, contrary to our results with maximum vertical aerosol transport in temperate dry winter regions, especially in the

Table 4. Pearson correlation coefficients for correlations between E_{UT}, $ELR_{1\,km}$, and $RCL_{0.5\,km}$, climate class resolved and for all MPCs (row All) for small (1.0 µm) and large (10.0 µm) aerosol tracers.

	E_{UT}: $ELR_{1\,km}$	$ELR_{1\,km}$: $RCL_{0.5\,km}$	E_{UT}: $RCL_{0.5\,km}$	E_{UT}: $ELR_{1\,km}$	$ELR_{1\,km}$: $RCL_{0.5\,km}$	E_{UT}: $RCL_{0.5\,km}$
1.0 µm	NS_{inact}			NS_{act}		
A	0.00	−0.26	−0.04	0.43	−0.31	−0.30
B	−0.97	0.43	−0.43	−0.76	−0.12	−0.36
Cf	−0.75	−0.38	−0.18	−0.61	−0.43	−0.31
Cs	−0.90	0.72	−0.88	−0.96	0.73	−0.84
Cw	−0.84	0.13	−0.60	−0.58	0.02	−0.70
D	−0.98	−0.92	0.84	−0.98	−0.95	0.86
All	−0.77	−0.19	−0.27	−0.51	−0.28	−0.49
10.0 µm	NS_{inact}			NS_{act}		
A	0.05	−0.31	−0.05	0.15	−0.38	−0.21
B	−0.92	0.39	−0.64	−0.59	−0.17	−0.63
Cf	−0.75	0.08	−0.53	−0.66	−0.09	−0.52
Cs	−0.96	0.89	−0.95	−0.97	0.90	−0.95
Cw	−0.70	0.22	−0.75	−0.49	0.09	−0.78
D	−0.97	0.45	−0.66	−0.92	0.01	−0.38
All	−0.74	0.13	−0.58	−0.50	−0.07	−0.66

case of NS_{act} means. The input of mass into the upper troposphere occurs in most cases by convective or conveyor belt lifting. Both processes are commonly associated with cloud formation and subsequent precipitation, which both remove aerosol particles efficiently. Nucleation scavenging during cloud formation is the dominant scavenging process for aerosol particles with diameters larger than 0.2 µm, while impaction scavenging becomes important for large aerosol particles. With sufficient lifting activity the E_{UT} mass fraction strongly depends on the liquid and/or ice water content of the clouds and their extension, which in turn determine the scavenged mass. From the pure gas-phase tracer simulations, we know that the upward transport is strongest in the tropics, though the moisture present there limits the upward transport of aerosols so strongly that less mass than in the temperate dry winter regions reaches the upper troposphere. In arid regions precipitation hardly affects lifting processes; however, the tracer distribution is affected by the development of a very deep, well-mixed air layer which can reach altitudes up to 5 km, such as the Saharan Air Layer (Hall and Peyrillé, 2007). The aerosols emitted at the surface are already mixed to altitudes of several kilometers in this layer, and consequent lifting above 5 km can occur faster and is often associated with little or no precipitation. Third, the seasonal cycle is also reversed compared to what was reported for $ELR_{1\,km}$, with minimum values during winter, overall mean of about 2 %, and maximum values during summer, overall mean between 4.5 and 6.5 % (see Fig. S4 in the Supplement). Furthermore, the variability, indicated by the standard deviation and also by the differences between various climate classes, is largest in summer and smallest in winter. This is again attributed to the convective activity, which is stronger in summer, but also shows strong differences between different regions of the world and thus also between different climate classes.

Thus, the interplay of atmospheric moisture and lifting activity and their effect on aerosol tracers is the determining factor for transport to the upper troposphere, with relatively small aerosol mass fractions in this domain.

4.3 Relation between pollution build-up and outflow

Finally, we want to see whether there are significant correlations between pollution build-up and outflow for aerosols from MPCs. L07 reported that for gas-phase tracers a significant relation was found, and that the upward transport, rather than the low-level transport, is mainly responsible for ventilating surface pollution. Moreover, they found that the trade-off between long-range low-level export and dilution of pollutants in the region surrounding the MPCs becomes more evident for regions with similar vertical transport.

In general, we find an anti-correlation between the horizontal and vertical export (see Table 4). This relationship is expected since aerosol mass is either lifted to higher altitudes or kept at lower levels, being advected rather horizontally. However, the overall anti-correlation is weakened by the weak positive correlation in the tropics. In the tropics, an ambiguous situation is found for different MPCs. For instance, in Jakarta and Manila the opposing relationship between the two export pathways is still assessed, while it breaks down in other MPCs, for instance in Rio de Janeiro, Kolkata, and Lagos. A possible interpretation might be that in

the first case convective scavenging dominates the wet deposition, and in the second case more aerosols are scavenged in large-scale clouds. In regions with dominant convective scavenging, more aerosol mass is effectively lifted to higher altitudes but also efficiently removed by scavenging. Less mass is then left over to participate in any long-range transport, especially at low levels. This could result in an opposing relationship between vertical and near-surface long-range transport. Oppositely, more large-scale scavenging indicates that a larger proportion of aerosol mass has possibly undergone farther transport before removal. A correlation between vertical and near-surface long-range transport would then suggest that the outflow occurs at high and low levels.

Between low-level export and low-level retention, the correlation coefficients show a very ambivalent behavior with most values in the range of $[-0.5, 0.5]$. The sign varies between various climate classes and also between aerosol size and solubility. Only in two cases are higher correlations assessed: a positive one in temperate dry summer regions for small and large aerosol tracers and a negative one for small aerosol tracers from cold regions. In the first region, the mass fraction is rather small for $\mathrm{RCL}_{0.5\,\mathrm{km}}$ but high for $\mathrm{ELR}_{1\,\mathrm{km}}$. The positive correlation indicates that the low-level export forms an important path to accumulate mass in the near-surface region downwind. A positive correlation might be expected for the cold regions with high $\mathrm{ELR}_{1\,\mathrm{km}}$ and $\mathrm{RCL}_{0.5\,\mathrm{km}}$ mass fraction. However, as the vertical export is low in this climate region, the strength of surface wind and turbulent mixing within the boundary layer determines whether more of the mass is retained close to the source or advected downwind.

As it is expected, the correlation coefficients between low-level retention and vertical export reveal in most cases a negative sign. For small aerosol tracers the correlations are rather weak; only in temperate dry summer regions do we see a strong anti-correlation and in cold regions a strong correlation. The positive correlation coefficients for cold regions reveal that if lifting takes place, it occurs close to the emission source at low levels. On the other hand, an anti-correlation points more to lifting that either takes place farther away from the source or has its origin above 500 m altitude. For most climate regions this is true for the large aerosol tracers as they show stronger anti-correlations, even in cold regions. However, the sampling statistics are small and not equally distributed over the climate classes, thus the results should only be interpreted as a first indication.

5 Aerosol–gas-phase comparison

Finally, to conclude the analysis of atmospheric dispersion from urban emission sources, we want to show similarities and differences between gas-phase tracers with a fixed atmospheric lifetime and aerosol tracers with various atmospheric residence times. Here, we mainly focus on aerosol tracers with a diameter of 1 µm which have a lifetime comparable to, though generally shorter than, the lifetime of the gas-phase tracers, but also include aerosol tracers with a diameter of 10 µm in parts of the discussion. In Sect. 3 we briefly discussed similarities and differences in the dispersion from MPCs with two different model systems. Now, we compare the aerosol results discussed in Sect. 4 with gas-phase tracer results from an EMAC simulation using the same configuration as used for the aerosol simulation.

Figure 3 gives a qualitative overview of how the atmospheric dispersion patterns change with respect to the removal of an atmospheric tracer. The amount of various removal processes acting on the individual tracers decreases from left to right in Fig. 3. In general, the gas-phase tracers in the right column are wider spread from the source due to their longer lifetime. Close to the source points, similar values are found for gas-phase and aerosol tracers, but farther away the discrepancies between the various types of tracers become more apparent. The total column densities reveal higher values in the direct outflow regions of the MPCs in the case of the gas-phase tracers and also in remote areas like the South Pacific with no significant tracer burden present for aerosol tracers. Tracer distributions in the surface layer vary strongly, and the transport to higher latitudes is not the strongest for the gas-phase tracers, but rather for $\mathrm{NS}_{\mathrm{inact}}$ tracers, especially in Northern Europe. In contrast, the gas-phase tracers predominate in the northern latitude storm tracks where almost no aerosol mass is simulated anymore. The largest differences between aerosol and gas-phase tracers are found for the column densities in the upper troposphere above 5 km. The absolute aerosol tracer peak values are about the magnitude of the background levels of the gas-phase tracers in remote areas. Moreover, location and strength of peak values differ, for instance for Khartoum and Teheran, which both have a much weaker signal in the gas phase compared to the background than for the aerosol tracers. Furthermore, Santiago and Lima are clearly discernible in the aerosol phase but not in the gas phase, and also the outflow from East Asia extends farther northward for the gas-phase tracers.

The question arises then how the pollution potentials differ between gas-phase and aerosol tracers. Figure 4 shows the three pollution potentials used to investigate the similarities and differences in the local pollution build-up and pollution export: $\mathrm{ELR}_{1\,\mathrm{km}}$ (top panel), E_{UT} (middle panel), and A_{10} (bottom panel). Generally, the accordance between aerosol and gas-phase tracers is higher when using the $\mathrm{NS}_{\mathrm{inact}}$ aerosols. The greatest similarity in pollution potential is found for the low-level pollution potentials. Aerosols show slightly higher $\mathrm{ELR}_{1\,\mathrm{km}}$ values than gas tracers, with coefficients of determination (R^2) higher than 0.9 ($\mathrm{NS}_{\mathrm{inact}}$) and 0.8 ($\mathrm{NS}_{\mathrm{act}}$), respectively. Since the R^2 are a measure of how much of the variance in the correlation can be explained by the source location, the tracer properties seem to be less important to determine the mass fraction found in the lowest layers downwind of the source. Instead, the

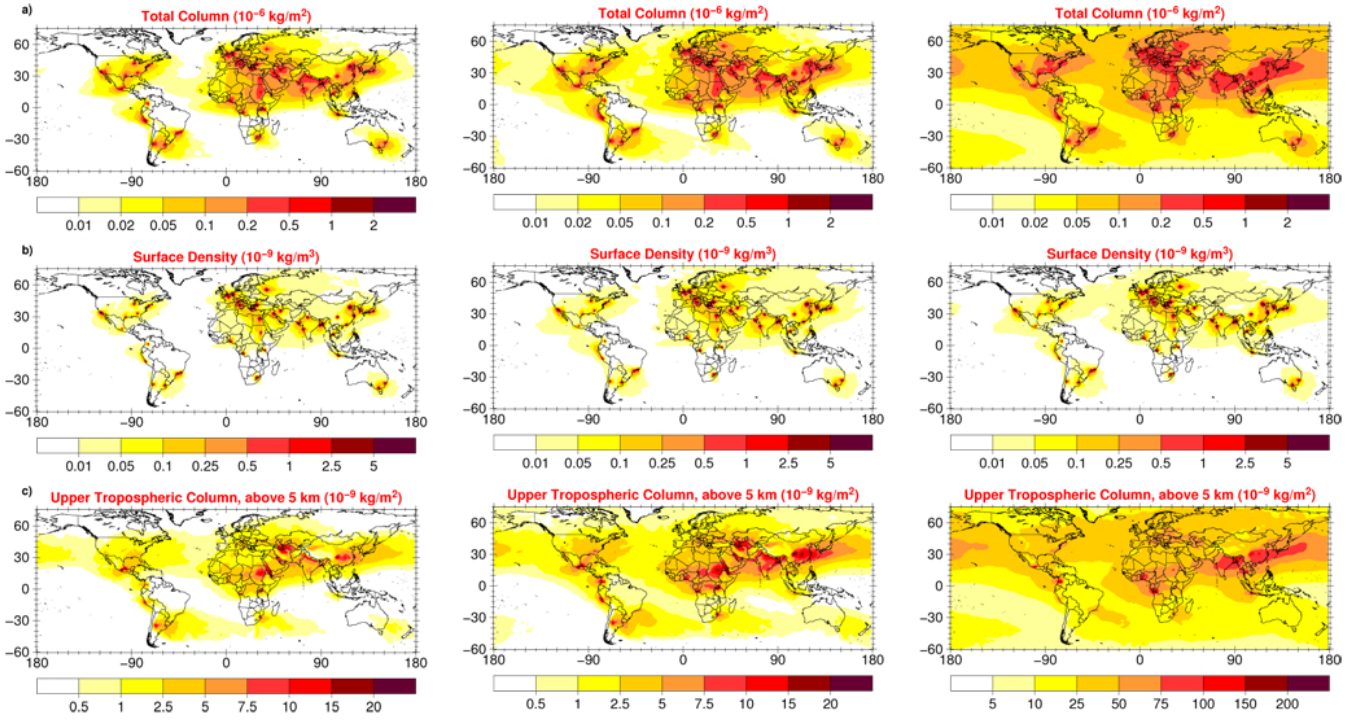

Fig. 3. Total column densities (top panel), surface densities (middle panel), and upper tropospheric column densities (bottom panel) for the sum of all 46 MPC tracer sources from the EMAC simulations. Left and central columns show the NS_{inact} and NS_{act} 1.0 µm aerosol tracers and the right column the gas-phase tracers with a 10 d decay lifetime. Units are 10^{-6} kg m^{-2} for total column densities, 10^{-9} kg m^{-3} for the surface densities, and 10^{-9} kg m^{-2} for the upper tropospheric column densities. Please note the different color-scaling, by a factor of ten, for the upper tropospheric column densities between the aerosol and gas-phase tracers.

location of the source along with the prevailing meteorology account for the mass transported downwind. In contrast, the vertical transport shows gas-phase mass fractions up to ten times higher than aerosol mass fractions. The correlation between gas and aerosol tracers is still positive but weak, with an R^2 of about 0.4 (NS_{inact}) and about 0.15 (NS_{act}), respectively. The source location is in this case of minor importance compared to the tracer properties, especially the solubility of a tracer, which determines to a great extent the mass fractions above 5 km. In the case of the area mass threshold exceedance, both the source location and tracer properties need to be considered more equally to explain the relation between gases and aerosols as positive correlations are found with $R^2 = 0.78$ (NS_{inact}) and $R^2 = 0.67$ (NS_{act}) for small aerosols and an averaged R^2 of about 0.53 for large aerosols. Hence, the source location determines the A_{10} more in the case of small aerosols, while the size of the aerosol seems to be more important for the large aerosols.

In summary, the findings of Sect. 4 are further supported by the comparison of gas-phase and aerosol tracers, especially that the source location is most important in determining the low-level pollution while tracer properties have a substantial impact on the vertical transport.

6 MPC impact on ecosystems and humans

Aerosol particles have the ability to potentially influence their environment when they are airborne in several ways. For instance, humans can breathe in small aerosol particles deeply into the lungs, and it is certain that this affects the life expectancy of humans (e.g., Dockery et al., 1993; Pope et al., 2009). Large particles are mainly responsible for decreasing visibility (e.g., Watson, 2002), and generally particles which contain toxic constituents from anthropogenic combustion can harm crops (e.g., Wiman et al., 1990; Burkhardt, 2010) and humans (e.g., Pöschl, 2005; Stanek et al., 2011). In this chapter we assess the potential impact of the urban emitted aerosol particles on the environment by using the metric D_X, which is the ratio of the total (= dry and wet) deposition flux to the global mean emission flux (defined in Sect. 2.2) and threshold values for X of 1 % and 5 %, and we refer to this as high relative deposition. Although we are aware of the different impacts of dry and wet deposited particles, we discuss only their sum here and leave a further investigation open for following studies. Furthermore, we use the metric A_Y to quantify the number of people that are exposed to a certain atmospheric mixing ratio.

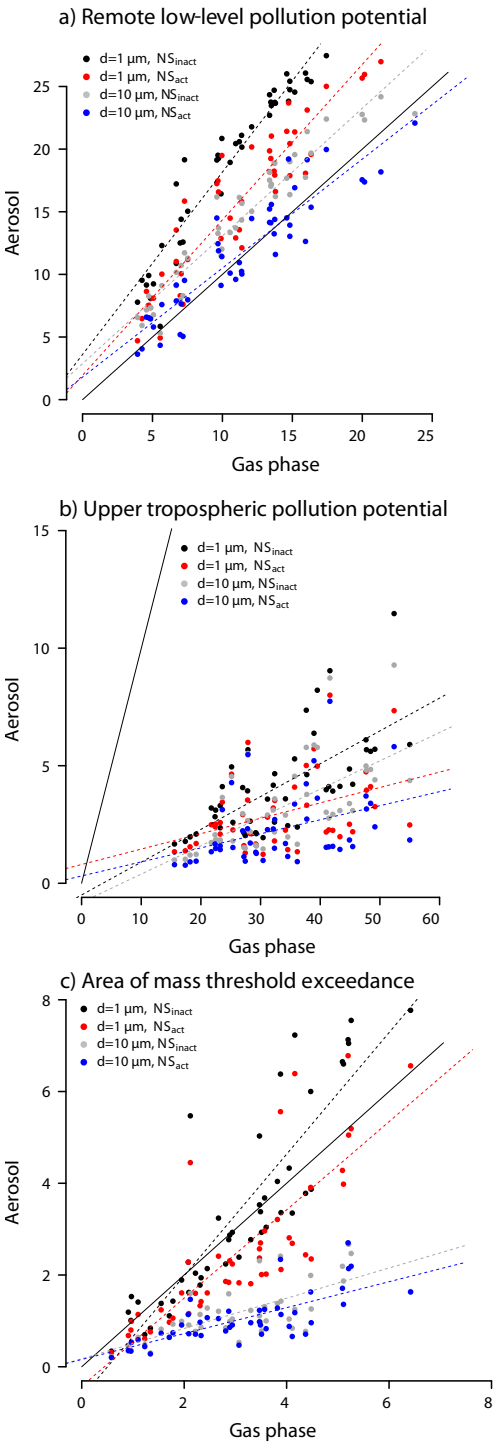

Fig. 4. Comparison between gas-phase and aerosol pollution potentials: ELR$_{1\,km}$ (top panel, in %), E_{UT} (middle panel, in %), and A_{10} (bottom panel, in 10^6 km^2). Colored dots represent different aerosol properties: black = NS$_{inact}$ 1.0 µm, red = NS$_{act}$ 1.0 µm, gray = NS$_{inact}$ 10.0 µm, and blue = NS$_{act}$ 10.0 µm. These aerosol tracers are considered to cover the aerosol spectrum of this study and other tracers are neglected to keep lucidity. The solid black lines represent the bisecting line, the colored dashed lines the regression lines (see equations in the Appendix).

6.1 Impact on ecosystems

6.1.1 Impact on land and sea surfaces

First, we assess the total surface area which fulfills the criterion of D_X. In Fig. 5 the total surface area is illustrated for each MPC for two aerosol diameters, 1.0 µm and 10.0 µm, on the left for D_1 and on the right for D_5. The solubility states are displayed by different gray shadings with the light gray bar representing the additional area between the two solubility states. In contrast to the atmospheric metrics, the smaller area, indicated by the dark gray bar, is not always determined by the same solubility state for each MPC, but most commonly by the NS$_{inact}$ tracers. If only a dark gray bar is drawn, then there is no difference between the two states, while a single light gray bar indicates that no area is covered at all for one state. By definition, areas which are covered with at least 5 % of the emissions are also covered with at least 1 %.

In the case of D_1, each MPC covers at least a small area, independent of aerosol size, which is not the case for D_5. Aerosol tracers from MPCs which are known to undergo substantial long-range transport, e.g., Baghdad, Teheran, Cairo, or Khartoum, are more widely spread and thus aerosol mass is deposited in lower concentrations in each grid cell. However, other MPCs, e.g., London or Tianjin, show also zero area covered, and thus long-range transport is not the only limiting factor for high relative deposition. In contrast, the maximum is found for MPCs which are either influenced by heavy precipitation rates, e.g., Lagos or MPCs in South East Asia, or located in a basin with low ventilation, e.g., Bogotá or Szechuan. On average, aerosol tracers with a diameter of 10.0 µm cover larger areas compared to the small aerosol tracers. The reason is that the large aerosol tracers travel shorter distances and the subsequent deposition occurs on smaller total overall area. Since the total global emitted mass is the same for each tracer, the deposition rates of the large aerosol tracers are in turn higher in the area where deposition occurs. Furthermore, the faster deposition rates for the large aerosols lead to smaller differences between the areas covered by the two solubility states.

Further, we divide the total surface area into land and sea fractions to obtain a more accurate knowledge over the location of high relative deposition. Generally, the low-level outflow of aerosols is similar to the gas-phase outflow reported by L07, with more low-level long-range transport over oceans. Nevertheless, the total deposition still occurs more over continents with about 55 % of the small tracer emissions and 68 % of the large tracer emissions being deposited on land surfaces. For the high relative deposition, we focus only on D_1 since not all of the MPCs cover a surface area in case of D_5. Since the land–sea fractionation is very similar for all aerosol tracers, independent of size or solubility, we choose the NS$_{act}$ 1.0 µm aerosol tracers to show D_1 in Fig. 6. The dark gray bars represent the land fraction which outweighs the sea fraction in the light gray color bars, although almost

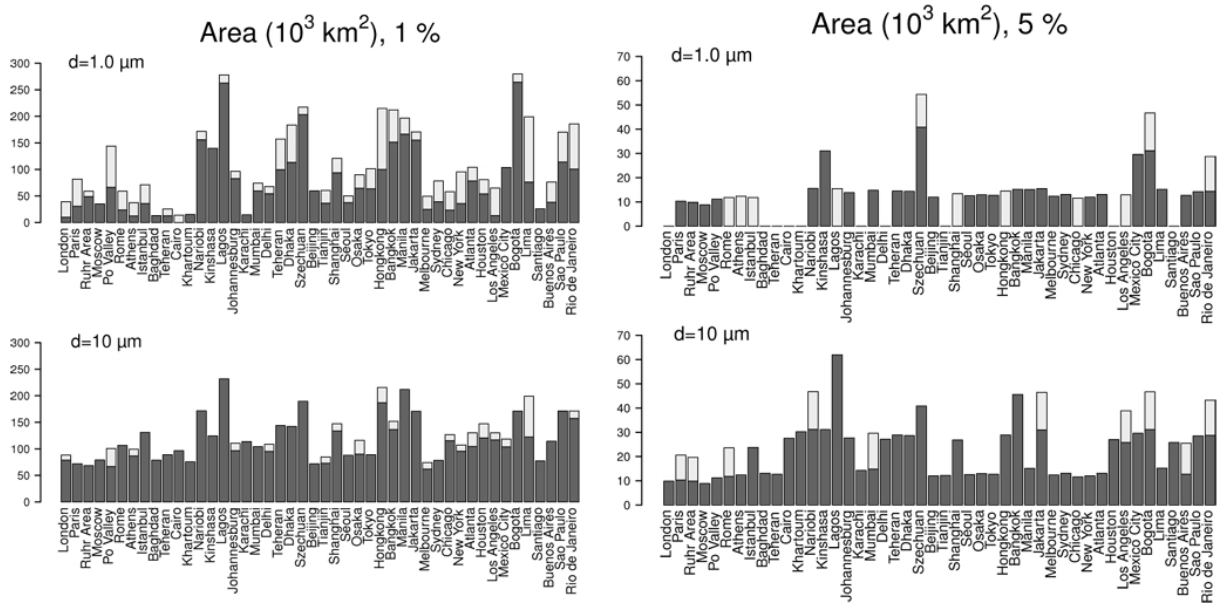

Fig. 5. Total area covered with more than 1 % (left side) and 5 % (right side) of the global mean annual emission. Top panels display the 1.0 µm aerosol tracers, and bottom panels the 10.0 µm aerosol tracers. The dark gray shaded bars show the minimum area covered by either the NS_{act} or NS_{inact} tracers, the light gray shaded bars on top the additional area covered by the tracers with the other nucleation scavenging state. Display order of the MPCs is by longitude, the area shown is in units of 10^3 km^2.

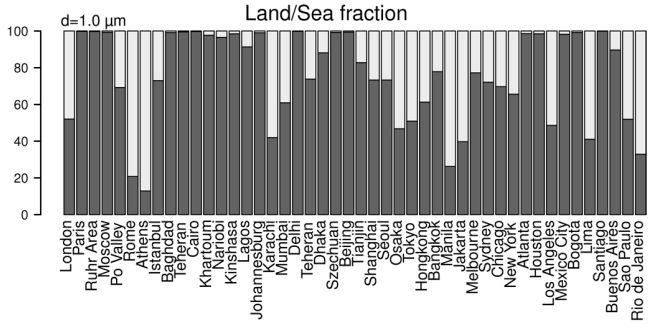

Fig. 6. Example for land–sea fractionation in % of D_1 for the NS_{act} 1.0 µm aerosol tracers. Dark gray bars represent the land fractions, light gray bars the sea fractions.

50 % of the MPCs are located at coastlines and several more close to the coast. In several cases the land fraction is close to 100 %, mainly for MPCs with a dominant outflow over continental regions, e.g., Moscow, Rhine–Ruhr area, Teheran, Delhi, and Szechuan. However, there are also some MPCs close to coastlines which do not have high relative deposition over seas, e.g., Santiago and Beijing. The highest marine D_1 values appear for Athens and Rome, with about 80 % sea fraction, but not surprisingly Jakarta and Manila show the highest sea fractions in terms of absolute area since each of these cities is located on a small island in a maritime environment.

6.1.2 Impact on cropland, pasture, and forest

To answer the question which of the three ecosystem – cropland, pasture, or forest – is most exposed to deposition from MPCs, we initially fold the sum of all annual accumulated MPC deposition fields with the relative fractions for cropland, pasture, and forest (see Fig. S1 in the Supplement). The differences between small aerosol tracers ($d \leq 1.0\,\mu m$) are minor as well as between the two solubility states. Thus, we focus the discussion on the NS_{act} 1.0 µm and 10.0 µm aerosol tracers, which are shown in Fig. 7. The pure deposition patterns have their maximum around the source location (Kunkel et al., 2012). In Fig. 7 MPCs are in most cases well detectable by the red areas in the six panels. For several MPCs these red areas exceed the MPC size since these are surrounded by large areas of an ecosystem, e.g., for cropland the corn-belt around Chicago, the region between Paris and east of the Rhine–Ruhr area, the region north of Lagos or large areas on the Indian subcontinent and in eastern China. In the case of pastureland, only a few hotspots are detected, for instance the region around Bogotá, the Sahel region in Africa, and again large areas in eastern China. Forests seem to be widely exposed to deposition from MPCs, e.g., in the USA in a belt from New England down to Atlanta, high forest deposition exposure is simulated, as well as in Bogotá and in the region between Rio de Janeiro and São Paulo. In Central Africa the Congo Basin with the African rainforest and in Asia regions in eastern China and also in Japan reveal high exposure. In Europe, the high northern latitudes are affected

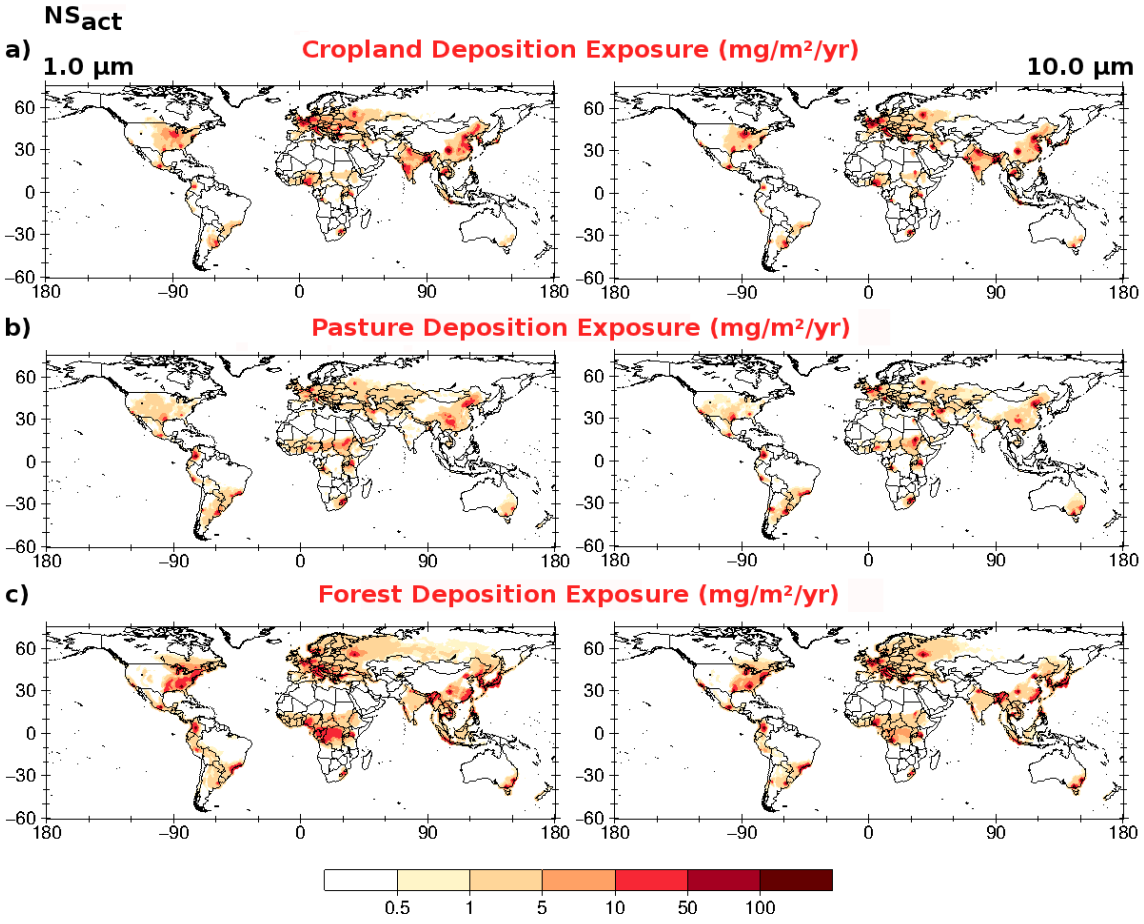

Fig. 7. Folded maps of the sum of all MPC annual accumulated deposition fields (in $\mathrm{mg\,m^{-2}\,yr^{-1}}$) and the relative fractions of the three ecosystems (see also Fig. S1 in the Supplement). The left side shows the $\mathrm{NS_{act}}$ 1.0 µm aerosol tracers, the right side the $\mathrm{NS_{act}}$ 10.0 µm aerosol tracers.

due to the vast appearance of boreal forest. For the same reason the deposition of Moscow can still be detected north of Mongolia far away from its source. In contrast, one of the most forested areas, the Amazon Basin, seems not to be affected by the deposition of the MPC tracers used in this study because it is not located downwind of the MPCs.

Using D_1 and D_5, we can calculate the area of each ecosystem which is exposed to more than 1% or 5% of the emission. Table 5 shows the averages of small and large aerosol tracers for each ecosystem. Generally, larger areas are found for the soluble tracers and, as discussed before for the total surface area, for larger aerosol tracers, with one exception in the case of forests for D_1 ($\mathrm{NS_{act}}$ 1.0 µm). The results for the two aerosol solubility states differ by less than 25%, in most cases even less than 20%. Maximum averages are found for forests, followed by croplands with up to 40% less and pasture with about 50% less area exposed to high relative deposition compared to forests. More detailed information for each MPC and ecosystem is found in Fig. S5 in the Supplement.

Table 5. Average area (in $10^3\,\mathrm{km^2}$) covered with high relative deposition, D_1 and D_5.

		Cropland	Pasture	Forest
D_1				
1.0 µm	$\mathrm{NS_{act}}$	20.26	12.61	33.21
	$\mathrm{NS_{inact}}$	16.37	10.74	31.23
10.0 µm	$\mathrm{NS_{act}}$	25.29	15.87	32.26
	$\mathrm{NS_{inact}}$	24.48	15.12	24.56
D_5				
1.0 µm	$\mathrm{NS_{act}}$	2.28	1.51	4.25
	$\mathrm{NS_{inact}}$	1.88	1.25	3.28
10.0 µm	$\mathrm{NS_{act}}$	5.29	3.14	6.54
	$\mathrm{NS_{inact}}$	4.69	2.60	5.85

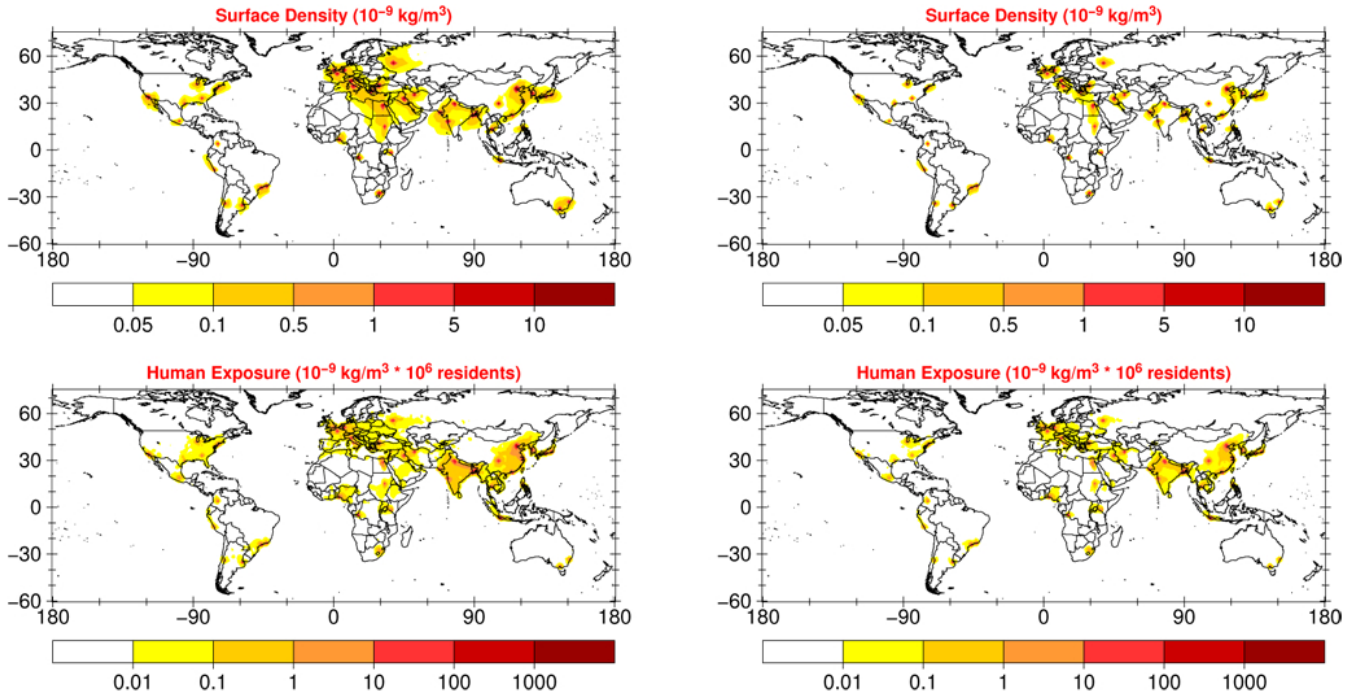

Fig. 8. Sum of all MPC surface densities in $10^{-9}\,\mathrm{kg\,m^{-3}}$ alone (upper panels) and convolved with the geographical population distribution (lower panels). The left side shows the NS_{act} 1.0 µm aerosol tracers, the right side the NS_{act} 10.0 µm aerosol tracers.

Taken together, forests which cover large areas on each continent are most affected by the MPC deposition. In contrast, pasture areas are also widespread, though they are less affected by the MPC deposition than croplands, which are mainly present in a few concentrated regions. However, these regions are nearly all close to or in the outflow regions of MPCs.

6.2 Population-based impact

We now assess the impact of MPC aerosols on humans. For this, surface densities are used instead of aerosol deposition fields, since airborne particles are potentially inhaled by humans and consequently cause health issues. Small aerosols are again represented by the 1.0 µm aerosol tracers, and for comparison and as an upper limit for efficiently inhalable aerosols we show also results for 10.0 µm aerosols.

Figure 8 displays surface densities in the upper panels for the NS_{act} tracers, on the left for the small aerosols (also shown in the middle panel in Fig. 3 with another color-scale), and on the right for the large aerosols. In the surface layer the differences between NS_{act} and NS_{inact} are almost negligible, especially in regions close to the MPCs, thus we focus our discussion on the NS_{act} aerosols tracers. The small aerosol tracers are commonly more widely dispersed due to the faster gravitational settling of large aerosols and subsequent removal out of the surface layer. MPCs are easily detectable by the red dots in the figure, even when the surface densities are convolved with the geographical population distribution (lower panels in Fig. 8). However, in addition two large domains are more accentuated: India and (East) China. Together these two countries host about one third of the global human population and thus the high population densities ensure that the highest numbers in the convolved variable of surface density and population distribution are found there. Other densely populated regions like Europe, Japan, or the Eastern US show similar surface densities but lower convolved numbers.

To further investigate and quantify how many people are affected by each MPC, we add up the number of people in the area with a mass threshold exceedance (A_Y). In Fig. 9 this is shown for the 1.0 µm and 10.0 µm aerosol tracers and a mass threshold Y of $10\,\mathrm{ng\,m^{-3}}$. The highest values are found independently of aerosol size or solubility in Delhi, Beijing, Tianjin, Karachi, and Shanghai, with more than 1.3 billion people being exposed to more than $10\,\mathrm{ng\,m^{-3}}$ in and around Delhi. For other MPCs like Sydney, Melbourne, Santiago, or Kinshasa, the lowest population numbers are found, simply due to the relatively sparse population density around these cities.

In conclusion, the area A_Y is a measure of the distribution of aerosol mass in the surface layer, especially of the dense part of the outflow plume. However, A_Y does not seem to determine how many people are exposed to a certain aerosol mass. Instead, this is more dependent on the population in and around an MPC. This is also underlined when computing the coefficients of determination to see how much of

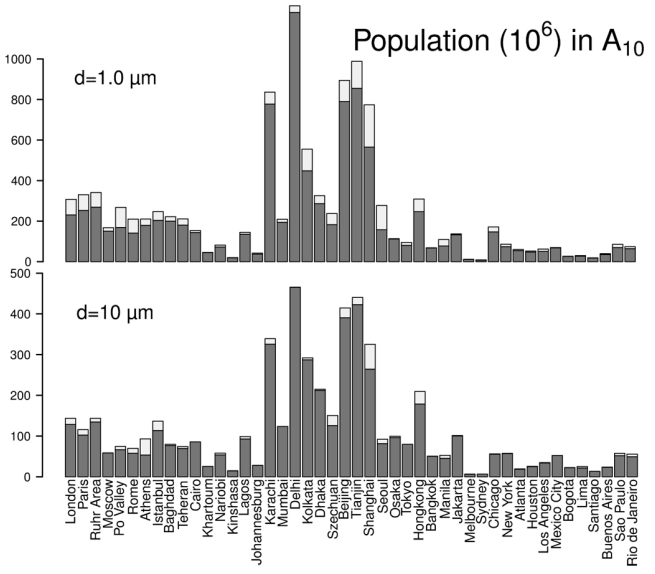

Fig. 9. Population in millions which reside in A_{10} for 1.0 µm (top panels) and 10.0 µm (bottom panels) aerosol tracers. Dark and light gray bars are defined as before.

the variance of the exposed population number is explicable by the area itself. For A_{10} we find only weak correlations for small ($R^2 < 0.2$) and large ($R^2 < 0.06$) aerosol tracers, and also by changing the threshold value to $1\,\mathrm{ng\,m^{-3}}$ and $100\,\mathrm{ng\,m^{-3}}$ we ascertain no substantially higher correlations.

7 Summary and conclusions

This study is an extension of Lawrence et al. (2007) to understand and compare the dispersion and deposition of air pollutants from urban centers. The primary focus is on generic aerosol tracers of five different monomodal sizes between 0.1 µm and 10.0 µm and two solubilities with various atmospheric residence times. In the AC-GCM EMAC ten tracers were released at each of the 46 different emission points, i.e., the major population centers considered in this study. The emission source strength is set to be equal for all tracers to obtain results only depending on prevailing meteorology and tracer properties.

We show that on average about 10–14 % of the emitted mass of aerosol tracers with diameters less than 2.5 µm (15–19 % for aerosols with diameters of 10.0 µm) is retained around the source. This number is highest in regions where pollutants have short atmospheric residence times, which are constrained by meteorological conditions, especially by scavenging in and below clouds, e.g., the tropics. Export from the cities, either by vertical mixing or low-level long-range transport, is determined by the stability of the atmosphere. High stability favors low-level export (on average between 12–20 % for the range of the different aerosol tracers) and is most dominant in cold regions, whereas the vertical export (on average 2.5–4 %) is strongest in regions with high lofting potential, i.e., high instability. Furthermore, the export to higher altitudes is dependent on the moisture in the atmosphere and therefore cloud formation and subsequent wet removal processes, which leads to the strongest export in temperate dry winter regions and not in tropical regions, in contrast to insoluble gas-phase tracers. The export at low levels is similar for aerosol and gas-phase tracers but substantially different for transport above 5 km, with gas-phase tracer concentrations up to ten times higher than the aerosol tracer concentrations due to the effective removal of aerosols in clouds. Moreover, the dispersion of generic gas-phase tracers from MPCs has been compared for two models, one with online calculated meteorology and one with semi-offline calculated meteorology as well as different physical parametrizations. These differences account for only about 25 % of the variance in the results; thus a high accordance is shown in vertical and long-range transport of the tracers between the two models.

Aerosol deposition fields convolved with geographical distributions of agricultural data and a metric to account for regions with high relative deposition are used to determine the impact of MPCs on ecosystems. We assess the area in which more than 1 % and 5 % of the emissions are deposited. On average the 10.0 µm aerosol tracers exceed these deposition fractions over larger areas with less variation between single MPCs than the aerosol tracers with smaller diameters. The areas vary more for smaller aerosols due to their longer lifetime and thus wider dispersion. This effect is strongest for MPCs in arid regions where aerosols have the longest atmospheric residence time while regions characterized by high precipitation or unfavorable geographic conditions reveal larger areas with high relative deposition. Most of this deposition occurs over land regions except for some MPCs like Rome, Athens, Jakarta, and Manila, with more deposition onto water surfaces. We further find that forests are more exposed to the aerosol deposition from MPCs than other land ecosystems such as cropland or pasture. Similarly, we use an area of mass threshold exceedance folded with population to assess the impact on humans and find that high population densities favor high human exposure, more so than the size of the area containing high surface mixing ratios.

All our results are solely based on model results and thus dependent on model uncertainties. The EMAC model was extensively evaluated for trace gas and aerosol distributions in many studies. A further improvement would be to represent the aerosol tracers better with properties, size and solubility, which can evolve in time and space and interact with other atmospheric constituents including clouds and atmospheric trace gases. This will be the scope of a follow-up study which investigates the impacts of different anthropogenic emissions from MPCs on the burdens of various aerosol types. Moreover, the coarse model resolution is a key issue with respect to the sub-grid-scale processes like the introduction of the emissions, vertical mixing, e.g., out of

the boundary layer, convection, or scavenging as these physical processes are of major importance for the distribution of tracers in the atmosphere. Higher vertical and horizontal resolution to better resolve small-scale circulation patterns can be provided either by regional-scale models or by Lagrangian dispersion models. However, regional-scale models have the limitation of many simulations being necessary to cover all the major population centers used in this study, while Lagrangian models have the advantage of having no numerical diffusion but lack in the representation of several tropospheric processes necessary to determine the distribution of trace gases and aerosols, e.g., convection, clouds, mixing, and scavenging. Nevertheless, since urban centers will become even more important in the future by serving as habitats for more people than at present, the research activities which have been accomplished so far, e.g., projects like MEGAPOLI (http://www.megapoli.info/, Baklanov et al., 2010), CityZEN (http://www.cityzen-project.eu/) and MILAGRO (http://www.eol.ucar.edu/projects/milagro/, Molina et al., 2010), should rather be seen as first initiatives which scratched the surface and provided initial results, but also left several questions open or created new questions.

Appendix A

Regression lines

In Fig. 4 regression lines are drawn. These regression lines are based on the following equations. x values are representatives of gas-phase results, y values of aerosol results.

For E_{UT}:

- $\mathrm{NS_{inact}}1.0\,\mu\mathrm{m}$: $y = 0.1392x - 0.4996$
- $\mathrm{NS_{act}}1.0\,\mu\mathrm{m}$: $y = 0.06542x + 0.79841$
- $\mathrm{NS_{inact}}10.0\,\mu\mathrm{m}$: $y = 0.1211x - 0.8125$
- $\mathrm{NS_{act}}10.0\,\mu\mathrm{m}$: $y = 0.06005x + 0.31090$

For $\mathrm{ELR_{1\,km}}$:

- $\mathrm{NS_{inact}}1.0\,\mu\mathrm{m}$: $y = 1.443x + 3.592$
- $\mathrm{NS_{act}}1.0\,\mu\mathrm{m}$: $y = 1.245x + 1.1950$
- $\mathrm{NS_{inact}}10.0\,\mu\mathrm{m}$: $y = 1.023x + 2.885$
- $\mathrm{NS_{act}}10.0\,\mu\mathrm{m}$: $y = 0.8722x + 1.8004$

For A_{10}:

- $\mathrm{NS_{inact}}1.0\,\mu\mathrm{m}$: $y = 1.352x - 0.6669$
- $\mathrm{NS_{act}}1.0\,\mu\mathrm{m}$: $y = 0.9642x - 0.4251$
- $\mathrm{NS_{inact}}10.0\,\mu\mathrm{m}$: $y = 0.3325x + 0.1759$
- $\mathrm{NS_{act}}10.0\,\mu\mathrm{m}$: $y = 0.2830x + 0.1589$

Supplementary material related to this article is available online at: http://www.atmos-chem-phys.net/13/4203/2013/acp-13-4203-2013-supplement.pdf.

Acknowledgements. The authors would like to thank all EMAC developers and modelers for providing code and helpful discussions. We further thank S. Borrmann for valuable advice and our MEGAPOLI partners for fruitful discussions. D. Kunkel acknowledges funding from the International Max Planck Research School. The open-source software packages Yorick (http://yorick.sourceforge.net/) and R (R Development Core Team, 2010) have been used for the analysis and graphics.

The service charges for this open access publication have been covered by the Max Planck Society.

Edited by: P. Stier

References

Baklanov, A., Lawrence, M., Pandis, S., Mahura, A., Finardi, S., Moussiopoulos, N., Beekmann, M., Laj, P., Gomes, L., Jaffrezo, J.-L., Borbon, A., Coll, I., Gros, V., Sciare, J., Kukkonen, J., Galmarini, S., Giorgi, F., Grimmond, S., Esau, I., Stohl, A., Denby, B., Wagner, T., Butler, T., Baltensperger, U., Builtjes, P., van den Hout, D., van der Gon, H. D., Collins, B., Schluenzen, H., Kulmala, M., Zilitinkevich, S., Sokhi, R., Friedrich, R., Theloke, J., Kummer, U., Jalkinen, L., Halenka, T., Wiedensholer, A., Pyle, J., and Rossow, W. B.: MEGAPOLI: concept of multi-scale modelling of megacity impact on air quality and climate, Adv. Sci. Res., 4, 115–120, doi:10.5194/asr-4-115-2010, 2010.

Betzer, P. R., Carder, K. L., Duce, R. A., Merrill, J. T., Tindale, N. W., Uematsu, M., Costello, D. K., Young, R. W., Feely, R. A., Breland, J. A., Bernstein, R. E., and Greco, A. M.: Long-range transport of giant mineral aerosol particles, Nature, 336, 568–571, doi:10.1038/336568a0, 1988.

Burkhardt, J.: Hygroscopic particles on leaves: nutrients or desiccants?, Ecol. Monogr., 80, 369–399, doi:10.1890/09-1988.1, WOS:000279801300002, 2010.

Burrows, S. M., Butler, T., Jöckel, P., Tost, H., Kerkweg, A., Pöschl, U., and Lawrence, M. G.: Bacteria in the global atmosphere – Part 2: Modeling of emissions and transport between different ecosystems, Atmos. Chem. Phys., 9, 9281–9297, doi:10.5194/acp-9-9281-2009, 2009.

Butler, T. M. and Lawrence, M. G.: The influence of megacities on global atmospheric chemistry: a modelling study, Environ. Chem., 6, 219–225, 2009.

Butler, T. M., Lawrence, M. G., Gurjar, B., van Aardenne, J., Schultz, M., and Lelieveld, J.: The representation of emissions from megacities in global emission inventories, Atmos. Environ., 42, 703–719, doi:10.1016/j.atmosenv.2007.09.060, 2008.

Butler, T. M., Stock, Z. S., Russo, M. R., Denier van der Gon, H. A. C., and Lawrence, M. G.: Megacity ozone air quality under four alternative future scenarios, Atmos. Chem. Phys., 12, 4413–4428, doi:10.5194/acp-12-4413-2012, 2012.

de Foy, B., Varela, J. R., Molina, L. T., and Molina, M. J.: Rapid ventilation of the Mexico City basin and regional fate of the urban plume, Atmos. Chem. Phys., 6, 2321–2335, doi:10.5194/acp-6-2321-2006, 2006.

Dee, D. P., Uppala, S. M., Simmons, A. J., Berrisford, P., Poli, P., Kobayashi, S., Andrae, U., Balmaseda, M. A., Balsamo, G., Bauer, P., Bechtold, P., Beljaars, A. C. M., van de Berg, L., Bidlot, J., Bormann, N., Delsol, C., Dragani, R., Fuentes, M., Geer, A. J., Haimberger, L., Healy, S. B., Hersbach, H., Hólm, E. V., Isaksen, L., Kållberg, P., Köhler, M., Matricardi, M., McNally, A. P., Monge-Sanz, B. M., Morcrette, J., Park, B., Peubey, C., de Rosnay, P., Tavolato, C., Thépaut, J., and Vitart, F.: The ERA-Interim reanalysis: configuration and performance of the data assimilation system, Q. J. Roy. Meteor. Soc., 137, 553–597, doi:10.1002/qj.828, 2011.

Dockery, D. W., Pope, C. A., Xu, X., Spengler, J. D., Ware, J. H., Fay, M. E., Ferris, B. G., and Speizer, F. E.: An association between air pollution and mortality in six US cities, New Engl. J. Med., 329, 1753–1759, doi:10.1056/NEJM199312093292401, 1993.

Duncan, B. N. and Bey, I.: A modeling study of the export pathways of pollution from Europe: seasonal and interannual variations (1987–1997), J. Geophys. Res., 109, D08301, doi:10.1029/2003JD004079, 2004.

Grimm, N. B., Faeth, S. H., Golubiewski, N. E., Redman, C. L., Wu, J., Bai, X., and Briggs, J. M.: Global change and the ecology of cities, Science, 319, 756–760, doi:10.1126/science.1150195, 2008.

Hall, N. M. and Peyrillé, P.: Dynamics of the West African monsoon, J. Phys. IV, 139, 81–99, doi:10.1051/jp4:2006139007, 2007.

Jaffe, D., Anderson, T., Covert, D., Kotchenruther, R., Trost, B., Danielson, J., Simpson, W., Berntsen, T., Karlsdottir, S., Blake, D., Harris, J., Carmichael, G., and Uno, I.: Transport of Asian air pollution to North America, Geophys. Res. Lett., 26, 711–714, 1999.

Jöckel, P., Sander, R., Kerkweg, A., Tost, H., and Lelieveld, J.: Technical Note: The Modular Earth Submodel System (MESSy) – a new approach towards Earth System Modeling, Atmos. Chem. Phys., 5, 433–444, doi:10.5194/acp-5-433-2005, 2005.

Jöckel, P., Tost, H., Pozzer, A., Brühl, C., Buchholz, J., Ganzeveld, L., Hoor, P., Kerkweg, A., Lawrence, M. G., Sander, R., Steil, B., Stiller, G., Tanarhte, M., Taraborrelli, D., van Aardenne, J., and Lelieveld, J.: The atmospheric chemistry general circulation model ECHAM5/MESSy1: consistent simulation of ozone from the surface to the mesosphere, Atmos. Chem. Phys., 6, 5067–5104, doi:10.5194/acp-6-5067-2006, 2006.

Jöckel, P., Kerkweg, A., Buchholz-Dietsch, J., Tost, H., Sander, R., and Pozzer, A.: Technical Note: Coupling of chemical processes with the Modular Earth Submodel System (MESSy) submodel TRACER, Atmos. Chem. Phys., 8, 1677–1687, doi:10.5194/acp-8-1677-2008, 2008.

Kalnay, E. and Cai, M.: Impact of urbanization and land-use change on climate, Nature, 423, 528–531, 2003.

Kerkweg, A., Buchholz, J., Ganzeveld, L., Pozzer, A., Tost, H., and Jöckel, P.: Technical Note: An implementation of the dry removal processes DRY DEPosition and SEDImentation in the Modular Earth Submodel System (MESSy), Atmos. Chem. Phys., 6, 4617–4632, doi:10.5194/acp-6-4617-2006, 2006a.

Kerkweg, A., Sander, R., Tost, H., and Jöckel, P.: Technical note: Implementation of prescribed (OFFLEM), calculated (ONLEM), and pseudo-emissions (TNUDGE) of chemical species in the Modular Earth Submodel System (MESSy), Atmos. Chem. Phys., 6, 3603–3609, doi:10.5194/acp-6-3603-2006, 2006b.

Kraas, F.: Megacities and global change: key priorities, Geogr. J., 173, 79–82, doi:10.1111/j.1475-4959.2007.232_2.x, 2007.

Kunkel, D., Lawrence, M. G., Tost, H., Kerkweg, A., Jöckel, P., and Borrmann, S.: Urban emission hot spots as sources for remote aerosol deposition, Geophys. Res. Lett., 39, L01808, doi:10.1029/2011GL049634, 2012.

Lawrence, M. G. and Rasch, P. J.: Tracer transport in deep convective updrafts: plume ensemble versus bulk formulations, J. Atmos. Sci., 62, 2880–2894, doi:10.1175/JAS3505.1, 2005.

Lawrence, M. G., Crutzen, P. J., Rasch, P. J., Eaton, B. E., and Mahowald, N. M.: A model for studies of tropospheric photochemistry: description, global distributions, and evaluation, J. Geophys. Res., 104, 26245–26277, 1999.

Lawrence, M. G., Butler, T. M., Steinkamp, J., Gurjar, B. R., and Lelieveld, J.: Regional pollution potentials of megacities and other major population centers, Atmos. Chem. Phys., 7, 3969–3987, doi:10.5194/acp-7-3969-2007, 2007.

Lelieveld, J., Kunkel, D., and Lawrence, M. G.: Global risk of radioactive fallout after major nuclear reactor accidents, Atmos. Chem. Phys., 12, 4245–4258, doi:10.5194/acp-12-4245-2012, 2012.

Lin, S. and Rood, R. B.: Multidimensional flux-form semi-lagrangian transport schemes, Mon. Weather Rev., 124, 2046–2070, doi:10.1175/1520-0493(1996)124<2046:MFFSLT>2.0.CO;2, 1996.

Liu, J. and Mauzerall, D. L.: Potential influence of inter-continental transport of sulfate aerosols on air quality, Environ. Res. Lett., 2, 045029, doi:10.1088/1748-9326/2/4/045029, 2007.

Liu, J., Mauzerall, D. L., Horowitz, L. W., Ginoux, P., and Fiore, A. M.: Evaluating inter-continental transport of fine aerosols: (1) Methodology, global aerosol distribution and optical depth, Atmos. Environ., 43, 4327–4338, doi:10.1016/j.atmosenv.2009.03.054, 2009.

Molina, L. T., Madronich, S., Gaffney, J. S., Apel, E., de Foy, B., Fast, J., Ferrare, R., Herndon, S., Jimenez, J. L., Lamb, B., Osornio-Vargas, A. R., Russell, P., Schauer, J. J., Stevens, P. S., Volkamer, R., and Zavala, M.: An overview of the MILAGRO 2006 Campaign: Mexico City emissions and their transport and transformation, Atmos. Chem. Phys., 10, 8697–8760, doi:10.5194/acp-10-8697-2010, 2010.

Molina, M. J. and Molina, L. T.: Megacities and atmospheric pollution, J. Air Waste Manage., 54, 644–680, 2004.

Monks, P., Granier, C., Fuzzi, S., Stohl, A., Williams, M., Akimoto, H., Amann, M., Baklanov, A., Baltensperger, U., Bey, I., Blake, N., Blake, R., Carslaw, K., Cooper, O., Dentener, F., Fowler, D., Fragkou, E., Frost, G., Generoso, S., Ginoux, P., Grewe, V., Guenther, A., Hansson, H., Henne, S., Hjorth, J., Hofzumahaus, A., Huntrieser, H., Isaksen, I., Jenkin, M., Kaiser, J., Kanakidou, M., Klimont, Z., Kulmala, M., Laj, P.,

Lawrence, M., Lee, J., Liousse, C., Maione, M., McFiggans, G., Metzger, A., Mieville, A., Moussiopoulos, N., Orlando, J., O'Dowd, C., Palmer, P., Parrish, D., Petzold, A., Platt, U., P öschl, U., Prévôt, A., Reeves, C., Reimann, S., Rudich, Y., Sellegri, K., Steinbrecher, R., Simpson, D., ten Brink, H., Theloke, J., van der Werf, G., Vautard, R., Vestreng, V., Vlachokostas, C. and von Glasow, R.: Atmospheric composition change – global and regional air quality, Atmos. Environ., 43, 5268–5350, doi:doi:10.1016/j.atmosenv.2009.08.021, 2009.

Nordeng, T.: Extended versions of the convective parametrization scheme at ECMWF and their impact on the mean and transient activity of the model in the tropics, Technical memorandum, ECMWF, Reading, UK, 1994.

Park, R. J., Jacob, D. J., Palmer, P. I., Clarke, A. D., Weber, R. J., Zondolo, M. A., Eisele, F. L., Bandy, A. R., Thornton, D. C., Sachse, G. W., and Bond, T. C.: Export efficiency of black carbon aerosol in continental outflow: global implications, J. Geophys. Res., 110, D11205, doi:10.1029/2004JD005432, 2005.

Parrish, D. D., Kuster, W. C., Shao, M., Yokouchi, Y., Kondo, Y., Goldan, P. D., de Gouw, J. A., Koike, M., and Shirai, T.: Comparison of air pollutant emissions among mega-cities, Atmos. Environ., 43, 6435–6441, doi:10.1016/j.atmosenv.2009.06.024, 2009.

Parrish, D. D., Singh, H. B., Molina, L., and Madronich, S.: Air quality progress in North American megacities: a review, Atmos. Environ., 45, 7015–7025, doi:10.1016/j.atmosenv.2011.09.039, 2011.

Peel, M. C., Finlayson, B. L., and McMahon, T. A.: Updated world map of the Köppen-Geiger climate classification, Hydrol. Earth Syst. Sci., 11, 1633–1644, doi:10.5194/hess-11-1633-2007, 2007.

Pope, C. A., Ezzati, M., and Dockery, D. W.: Fine-particulate air pollution and life expectancy in the United States, New Engl. J. Med., 360, 376–386, doi:10.1056/NEJMsa0805646, 2009.

Pöschl, U.: Atmospheric aerosols: composition, transformation, climate and health effects, Angew. Chem. Int. Edit., 44, 7520–7540, doi:10.1002/anie.200501122, 2005.

Pozzer, A., Jöckel, P., and Van Aardenne, J.: The influence of the vertical distribution of emissions on tropospheric chemistry, Atmos. Chem. Phys., 9, 9417–9432, doi:10.5194/acp-9-9417-2009, 2009.

Pozzer, A., Pollmann, J., Taraborrelli, D., Jöckel, P., Helmig, D., Tans, P., Hueber, J., and Lelieveld, J.: Observed and simulated global distribution and budget of atmospheric C_2-C_5 alkanes, Atmos. Chem. Phys., 10, 4403–4422, doi:10.5194/acp-10-4403-2010, 2010.

Pozzer, A., de Meij, A., Pringle, K. J., Tost, H., Doering, U. M., van Aardenne, J., and Lelieveld, J.: Distributions and regional budgets of aerosols and their precursors simulated with the EMAC chemistry-climate model, Atmos. Chem. Phys., 12, 961–987, doi:10.5194/acp-12-961-2012, 2012.

Pringle, K. J., Tost, H., Pozzer, A., Pöschl, U., and Lelieveld, J.: Global distribution of the effective aerosol hygroscopicity parameter for CCN activation, Atmos. Chem. Phys., 10, 5241–5255, doi:10.5194/acp-10-5241-2010, 2010.

Ramankutty, N., Evan, A. T., Monfreda, C., and Foley, J. A.: Farming the planet: 1. Geographic distribution of global agricultural lands in the year 2000, Global Biogeochem. Cy., 22, GB1003, doi:10.1029/2007GB002952, 2008.

Rasch, P. J., Mahowald, N. M., and Eaton, B. E.: Representations of transport, convection, and the hydrologic cycle in chemical transport models: implications for the modeling of short-lived and soluble species, J. Geophys. Res., 102, 28127–28138, doi:10.1029/97JD02087, 1997.

R Development Core Team: R: A Language and Environment for Statistical Computing, R Foundation for Statistical Computing, Vienna, 2010.

Roeckner, E., Brokopf, R., Esch, M., Giorgetta, M., Hagemann, S., Kornblueh, L., Manzini, E., Schlese, U., and Schulzweida, U.: Sensitivity of simulated climate to horizontal and vertical resolution in the ECHAM5 atmosphere model, J. Climate, 19, 3771–3791, doi:10.1175/JCLI3824.1, 2006.

Seinfeld, J. H. and Pandis, S. N.: Atmospheric Chemistry and Physics – From Air Pollution to Climate Change, 2nd Edn., John Wiley & Sons. Inc, Hoboken, New Jersey, 2006.

Socioeconomic Data and Appliaction Center (SEDAC): Gridded Population of the World Version 3 (GPWv3), Columbia University, Palisades, NY, USA, available at: http://sedac.ciesin.columbia.edu/gpw (last access: 4 April 2011), 2005.

Song, J., Lei, W., Bei, N., Zavala, M., de Foy, B., Volkamer, R., Cardenas, B., Zheng, J., Zhang, R., and Molina, L. T.: Ozone response to emission changes: a modeling study during the MCMA-2006/MILAGRO Campaign, Atmos. Chem. Phys., 10, 3827–3846, doi:10.5194/acp-10-3827-2010, 2010.

Stanek, L. W., Sacks, J. D., Dutton, S. J., and Dubois, J. B.: Attributing health effects to apportioned components and sources of particulate matter: an evaluation of collective results, Atmos. Environ., 45, 5655–5663, doi:10.1016/j.atmosenv.2011.07.023, 2011.

Stohl, A., Eckhardt, S., Forster, C., James, P., and Spichtinger, N.: On the pathways and timescales of intercontinental air pollution transport, J. Geophys. Res., 107, 4684, doi:10.1029/2001JD001396, 2002.

Stohl, A., Huntrieser, H., Richter, A., Beirle, S., Cooper, O. R., Eckhardt, S., Forster, C., James, P., Spichtinger, N., Wenig, M., Wagner, T., Burrows, J. P., and Platt, U.: Rapid intercontinental air pollution transport associated with a meteorological bomb, Atmos. Chem. Phys., 3, 969–985, doi:10.5194/acp-3-969-2003, 2003.

Streets, D. G., Fu, J. S., Jang, C. J., Hao, J., He, K., Tang, X., Zhang, Y., Wang, Z., Li, Z., Zhang, Q., Wang, L., Wang, B., and Yu, C.: Air quality during the 2008 Beijing Olympic Games, Atmos. Environ., 41, 480–492, doi:10.1016/j.atmosenv.2006.08.046, 2007.

Tiedtke, M.: A comprehensive mass flux scheme for cumulus parameterization in large-scale models, Mon. Weather Rev., 117, 1779–1800, 1989.

Tost, H., Jöckel, P., Kerkweg, A., Sander, R., and Lelieveld, J.: Technical note: A new comprehensive SCAVenging submodel for global atmospheric chemistry modelling, Atmos. Chem. Phys., 6, 565–574, doi:10.5194/acp-6-565-2006, 2006.

Tost, H., Jöckel, P., Kerkweg, A., Pozzer, A., Sander, R., and Lelieveld, J.: Global cloud and precipitation chemistry and wet deposition: tropospheric model simulations with ECHAM5/MESSy1, Atmos. Chem. Phys., 7, 2733–2757, doi:10.5194/acp-7-2733-2007, 2007.

Tost, H., Lawrence, M. G., Brühl, C., Jöckel, P., The GABRIEL Team, and The SCOUT-O3-DARWIN/ACTIVE Team: Uncertainties in atmospheric chemistry modelling due to convection

parameterisations and subsequent scavenging, Atmos. Chem. Phys., 10, 1931–1951, doi:10.5194/acp-10-1931-2010, 2010.

UNFPA: State of World Population 2007: Unleashing the Potential of Urban Growth, New York, 2007.

von Kuhlmann, R., Lawrence, M. G., Crutzen, P. J., and Rasch, P. J.: A model for studies of tropospheric ozone and nonmethane hydrocarbons: model description and ozone results, J. Geophys. Res., 108, 4729, doi:10.1029/2002JD003348, 2003.

Wagstrom, K. M. and Pandis, S. N.: Source-receptor relationships for fine particulate matter concentrations in the Eastern United States, Atmos. Environ., 45, 347–356, doi:10.1016/j.atmosenv.2010.10.019, 2010.

Wang, T., Nie, W., Gao, J., Xue, L. K., Gao, X. M., Wang, X. F., Qiu, J., Poon, C. N., Meinardi, S., Blake, D., Wang, S. L., Ding, A. J., Chai, F. H., Zhang, Q. Z., and Wang, W. X.: Air quality during the 2008 Beijing Olympics: secondary pollutants and regional impact, Atmos. Chem. Phys., 10, 7603–7615, doi:10.5194/acp-10-7603-2010, 2010.

Watson, J. G.: Visibility: science and regulation, J. Air Waste Manage., 52, 628–713, 2002.

Wild, O. and Akimoto, H.: Intercontinental transport of ozone and its precursors in a three-dimensional global CTM, J. Geophys. Res., 106, 27729–27744, 2001.

Wiman, B. L., Unsworth, M. H., Lindberg, S. E., Bergkvist, B., Jaenicke, R., and Hansson, H.-C.: Perspectives on aerosol deposition to natural surfaces: interactions between aerosol residence times, removal processes, the biosphere and global environmental change, J. Aerosol Sci., 21, 313–338, doi:10.1016/0021-8502(90)90051-X, 1990.